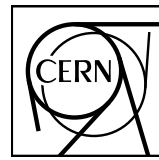


EUROPEAN ORGANIZATION FOR NUCLEAR RESEARCH



ALICE

CERN-EP-2023-195
30 August 2023

Multiplicity and event-scale dependent flow and jet fragmentation in pp collisions at $\sqrt{s} = 13$ TeV and in p–Pb collisions at $\sqrt{s_{\text{NN}}} = 5.02$ TeV

ALICE Collaboration*

Abstract

Long- and short-range correlations for pairs of charged particles are studied via two-particle angular correlations in pp collisions at $\sqrt{s} = 13$ TeV and p–Pb collisions at $\sqrt{s_{\text{NN}}} = 5.02$ TeV. The correlation functions are measured as a function of relative azimuthal angle $\Delta\phi$ and pseudorapidity separation $\Delta\eta$ for pairs of primary charged particles within the pseudorapidity interval $|\eta| < 0.9$ and the transverse-momentum interval $1 < p_{\text{T}} < 4 \text{ GeV}/c$. Flow coefficients are extracted for the long-range correlations ($1.6 < |\Delta\eta| < 1.8$) in various high-multiplicity event classes using the low-multiplicity template fit method. The method is used to subtract the enhanced yield of away-side jet fragments in high-multiplicity events. These results show decreasing flow signals toward lower multiplicity events. Furthermore, the flow coefficients for events with hard probes, such as jets or leading particles, do not exhibit any significant changes compared to those obtained from high-multiplicity events without any specific event selection criteria. The results are compared with hydrodynamic-model calculations, and it is found that a better understanding of the initial conditions is necessary to describe the results, particularly for low-multiplicity events.

© 2023 CERN for the benefit of the ALICE Collaboration.

Reproduction of this article or parts of it is allowed as specified in the CC-BY-4.0 license.

*See Appendix A for the list of collaboration members

1 Introduction

High-energy nucleus–nucleus (AA) collisions exhibit strong collectivity, which has been observed through anisotropy in the momentum distribution of emitted final-state particles at RHIC [1–4] and the LHC [5–8]. This momentum anisotropy is developed by the pressure-driven expansion of the strongly interacting quark–gluon plasma (QGP), which emerges from the initial spatial anisotropy in such collisions. The collective nature of the momentum anisotropy is mostly deduced via particle correlations which span over a wide range of pseudorapidity. The collective motion of the emitted particles, which reflects the collectivity of the initial medium, is generally quantified using a Fourier expansion, characterizing the so-called “anisotropic flow” [9]. In recent years, long-range correlations have been also observed in smaller collision systems such as high-multiplicity proton–proton (pp) [10–16], proton–nucleus (pA) [17–20], and in collisions of light nuclei [21, 22]. These observations raise the question to what extent do small-system collisions and heavy-ion collisions share the underlying mechanism, which is responsible for the observed long-range correlations. A crucial evidence of a strongly interacting medium in small-system collisions would be the presence of jet quenching [23, 24]. However, this phenomenon has not yet been observed in either high-multiplicity pp or p–Pb collisions [25–29], possibly due to the current experimental uncertainties being too large to observe it in such small-system collisions.

Current approaches to model heavy-ion collisions divide the evolution of the out-of-equilibrium, strongly-coupled, quantum-chromodynamic medium into multiple stages, and each stage is described by an effective theory. To this date, the combination of color-glass condensate effective field theory (CGC-EFT) [30, 31], causal hydrodynamics [32–40], and a hadronic cascade model [41–43] leads to the most successful description of a wide range of observables in heavy-ion collisions, e.g., particle spectra, centrality dependence of average particle transverse momenta, and multi-particle correlations [44–51]. By employing global Bayesian analyses, parameters of the multi-stage model, including those quantifying the transport properties of the QGP, can be constrained using measured data [52–55]. Despite the studies describing both heavy AA and pA collisions in a single framework [56], the origin of the flow-like correlations is still under debate. It is unclear whether the flow-like behavior originates from the early stages of the collision in the realm of applicability of CGC-EFT [57, 58] or whether it develops during the collective evolution, where causal hydrodynamics is applicable [59, 60]. Both scenarios may be responsible for the observed correlations in the final state [59]. Although collective models are successful in describing available two-particle correlation data from small-system collisions, they predict the opposite sign for four-particle azimuthal cumulants compared to experiment [12, 14, 61]. On the other hand, a semi-analytical toy model based on the Gubser hydrodynamic solution [62, 63] can explain the two- and four-particle correlations in pp collisions [64]. In particular, this model has explained the relationship between the sign of the four-particle cumulants and fluctuations in the initial state [64].

Besides the models based on the causal hydrodynamic framework, there are other attempts to explain the observed flow-like signals in small-system collisions using alternative descriptions. For instance, a study based on the A Multi-Phase Transport model (AMPT) [65] leads to satisfactory agreement with the experimental data [66]. The applicability of fluid-dynamical simulations and partonic cascade models in small-system collisions was explored in Ref. [67]. In a kinetic-theory framework with isotropization-time approximation, it is possible to explain the long-range correlations by fluid-like (hydrodynamic) excitation for Pb–Pb collisions and particle-like (or non-hydrodynamic) excitation for pp or p–Pb collisions [68–70]. Another potential description for the collectivity in small-system collisions is provided by PYTHIA 8, in which interacting strings repel one another in a transverse direction by a mechanism dubbed as “string shoving” [71, 72]. The repulsion of the strings causes microscopic transverse pressure, giving rise to long-range correlations of particles. The string shoving approach in PYTHIA 8 successfully reproduces the near-side ridge yield observed in measurements by ALICE [73] and CMS [12]. A systematic mapping of correlation effects across collision systems of various sizes is currently underway on the theoretical side, for example, see Ref. [74]. A quantitative description of the full set of experi-

mental data has not been achieved yet. A summary of various explanations for the observed correlations in small-system collisions is given in Refs. [75–77].

Measurements of anisotropic flow in small-system collisions are strongly affected by non-flow effects, predominantly originating from correlations among the constituents of jet fragmentation processes. In case of two-particle correlations, the non-flow contribution is usually suppressed by requiring a large $\Delta\eta$ gap between the two particles. This separation in pseudorapidity is also widely used in cumulant methods [13, 78]. However, this $\Delta\eta$ -gap method removes the non-flow contribution only on the near side ($\Delta\phi \sim 0$) and not on the away side ($\Delta\phi \sim \pi$). Later, a low-multiplicity template fit method was proposed to remove non-flow contributions on the away-side [10, 19, 79]. This method takes into account that the yield of jet fragments increases with increasing particle multiplicity [80–82]. By using the template fit method, the yield of away-side jet fragments can be subtracted, provided that the distribution that quantifies the shape of jet fragments is independent of the multiplicity class and therefore can be described by the low-multiplicity template.

As an extension of the studies of the near-side long-range ridge and jet-fragmentation yields in pp collisions at the center-of-mass energy $\sqrt{s} = 13$ TeV [73] and in p–Pb collisions at the center-of-mass energy per nucleon pair $\sqrt{s_{\text{NN}}} = 5.02$ TeV [17, 83], this article studies the interplay of jet production and collective effects, i.e., short- and long-range correlations simultaneously in these systems. The article also reports flow coefficients extracted for collisions tagged with different event-scale selections. The event-scale selection requires a minimum transverse momentum of the leading particle or the reconstructed jet at midrapidity, which is expected to bias the impact parameter of pp collisions to be smaller on average [84–86]. At the same time, the transverse momentum of the leading particle or the reconstructed jet provides a measure of the four-momentum transfer (Q^2) in the hard-parton scattering [87–89]. The transverse-momentum threshold implies a higher Q^2 for the collision. Such events with a large Q^2 may, on average, have a lower impact parameter than pp events without any requirement on Q^2 [85].

This article is organized as follows. First, the experimental setup and analysis method are described in Sec. 2 and Sec. 3, respectively. Section 4 discusses the systematic uncertainties. The results and their comparison with model calculations are presented and discussed in Sec. 5. Finally, the results are summarized in Sec. 6.

2 Experimental setup and data samples

The analysis is based on pp and p–Pb data collected during the LHC Run 2 period. The pp collisions had a center-of-mass energy $\sqrt{s} = 13$ TeV, and they were recorded from 2016 to 2018. The p–Pb collisions had a center-of-mass energy per nucleon–nucleon pair $\sqrt{s_{\text{NN}}} = 5.02$ TeV, and they were collected in 2016. It is worth noting that in p–Pb collisions there is a shift in the center-of-mass rapidity of $\Delta y = 0.465$ in the direction of the proton beam due to the asymmetric collision system.

A comprehensive description of the ALICE detector and its performance can be found in Refs. [8, 90, 91]. The analysis utilizes the V0 detector [92], the Inner Tracking System (ITS) [93, 94], and the Time Projection Chamber (TPC) [95].

The V0 detector consists of two stations on both sides of the interaction point, V0A and V0C, each comprising 32 plastic scintillator tiles, covering the full azimuthal angle within the pseudorapidity intervals $2.8 < \eta < 5.1$ and $-3.7 < \eta < -1.7$, respectively. The ITS is a silicon tracker with six layers of silicon sensors. The two innermost layers of the ITS are called the Silicon Pixel Detector (SPD) [96]. In addition to the two SPD layers, the middle two layers are the Silicon Drift Detector, and the outermost layers are the Silicon Strip Detector. The TPC is a gas-filled cylindrical tracking detector providing up to 159 reconstruction points for charged tracks traversing the full radial extent of the detector.

The V0 provides a minimum bias (MB) trigger in both pp and p–Pb collisions and an additional high-

multiplicity trigger in pp collisions. The MB trigger is obtained by a time coincidence of V0A and VOC signals. Amplitudes of V0A and VOC signals are proportional to charged-particle multiplicity, and their sum is denoted as V0M. The high-multiplicity trigger in pp collisions requires the V0M signal to exceed five times the mean value measured in MB collisions, selecting the 0.1% of MB events with the largest V0M multiplicity. The centrality in p–Pb collisions is determined using the V0A detector, which is located in the Pb-going direction [25]. The analyzed data samples of MB and high-multiplicity pp events at $\sqrt{s} = 13$ TeV correspond to integrated luminosities (\mathcal{L}_{int}) of about 19 nb^{-1} and 11 pb^{-1} , respectively [97]. In p–Pb collisions at $\sqrt{s_{\text{NN}}} = 5.02$ TeV, the corresponding integrated luminosity is $\mathcal{L}_{\text{int}} \sim 0.3 \text{ nb}^{-1}$.

Positions of primary vertices are reconstructed from signals measured by the SPD. The reconstructed primary vertices are required to be within 8 cm of the nominal interaction point along the beam direction. Pileup events are identified as events with multiple reconstructed primary vertices. These events are rejected if the distance between any of the vertices to the main primary vertex is greater than 0.8 cm. The probability of pileup events is estimated to range from 10^{-3} to 10^{-2} for MB and high-multiplicity events in pp collisions [98]. The pileup probability is estimated to be negligible in p–Pb collisions [29].

Charged-particle tracks are reconstructed using the combined information from the ITS and TPC. For charged particles emitted from a vertex located within $|z_{\text{vtx}}| < 8$ cm along the beam direction, the ITS and TPC provide a pseudorapidity coverage of $|\eta| < 1.4$ and 0.9, respectively. Both detectors have full coverage in azimuth. They are placed in a uniform magnetic field of 0.5 T that is oriented along the beam direction.

The charged-particle selection criteria are optimized to ensure a uniform efficiency over the midrapidity range $|\eta| < 0.9$ to mitigate the effects of small areas where some ITS layers are inactive in both collision systems. The selected sample of tracks consists of two classes. Tracks in the first class must have at least one hit in the SPD. Tracks of the second class do not have any hits in the SPD, but their origin is constrained to the primary vertex [17]. Charged-particle tracks are reconstructed down to a transverse momentum (p_T) of 0.15 GeV/c with an efficiency of approximately 65% [99]. The efficiency increases to 80% for particles with $p_T > 1$ GeV/c. The p_T resolution is approximately 1% for primary charged particles [100] with $p_T < 1$ GeV/c, and it linearly increases to 6% at $p_T \sim 50$ GeV/c in pp collisions and 10% in p–Pb collisions [101].

3 Analysis procedure

3.1 Two-particle angular correlations

Two-particle angular correlations are measured as a function of the relative azimuthal angle ($\Delta\phi$) and the relative pseudorapidity ($\Delta\eta$) between a trigger and associated particles

$$\frac{1}{N_{\text{trig}}} \frac{d^2N_{\text{pair}}}{d\Delta\eta d\Delta\phi} = B(0,0) \frac{S(\Delta\eta, \Delta\phi)}{B(\Delta\eta, \Delta\phi)} \Big|_{p_{T,\text{trig}}, p_{T,\text{assoc}}}, \quad (1)$$

where $p_{T,\text{trig}}$ and $p_{T,\text{assoc}}$ denote the transverse momentum of the trigger and associated particles, respectively. While the transverse momentum range for associated particles is fixed to $1 < p_{T,\text{assoc}} < 4$ GeV/c for trigger particles, several transverse momentum ranges are considered. The lower limit of $p_{T,\text{trig}}$ and $p_{T,\text{assoc}}$ (> 1 GeV/c) is chosen in order to avoid jet-like contributions from lower p_T particles which extend into the larger $\Delta\eta$ range because of the limited η acceptance [73]. The numbers of trigger particles and trigger-associated particle pairs are denoted as N_{trig} and N_{pair} , respectively. The average number of pairs in the same event, denoted by $S(\Delta\eta, \Delta\phi)$, is given by $\frac{1}{N_{\text{trig}}} \frac{d^2N_{\text{same}}}{d\Delta\eta d\Delta\phi}$. The $B(\Delta\eta, \Delta\phi)$ represents the number of pairs in mixed events and is normalized with its value at the point where $\Delta\eta = 0$ and $\Delta\phi = 0$, denoted as $B(0,0)$. To correct for acceptance effects, $S(\Delta\eta, \Delta\phi)$ is divided by $B(\Delta\eta, \Delta\phi)/B(0,0)$. The particles are weighted by the inverse of the tracking efficiency, which is obtained in the same way as

in Ref. [73]. In that study, the tracking efficiency and the secondary contamination (fake rate) were calculated using a detector simulation with the PYTHIA 8 event generator and the GEANT3 transport code [102]. To account for differences in particle composition between real data and PYTHIA, the tracking efficiency is determined from the above mentioned PYTHIA-based simulation with reweighted primary particle-species composition. The weights reflect realistic abundances of different particle species, which were extracted by a data-driven method [101, 103]. Events to be mixed are required to have primary vertices within the same 2 cm wide z_{vtx} interval. The correlation functions are averaged over the vertex intervals, resulting in the final per-trigger yield [104, 105].

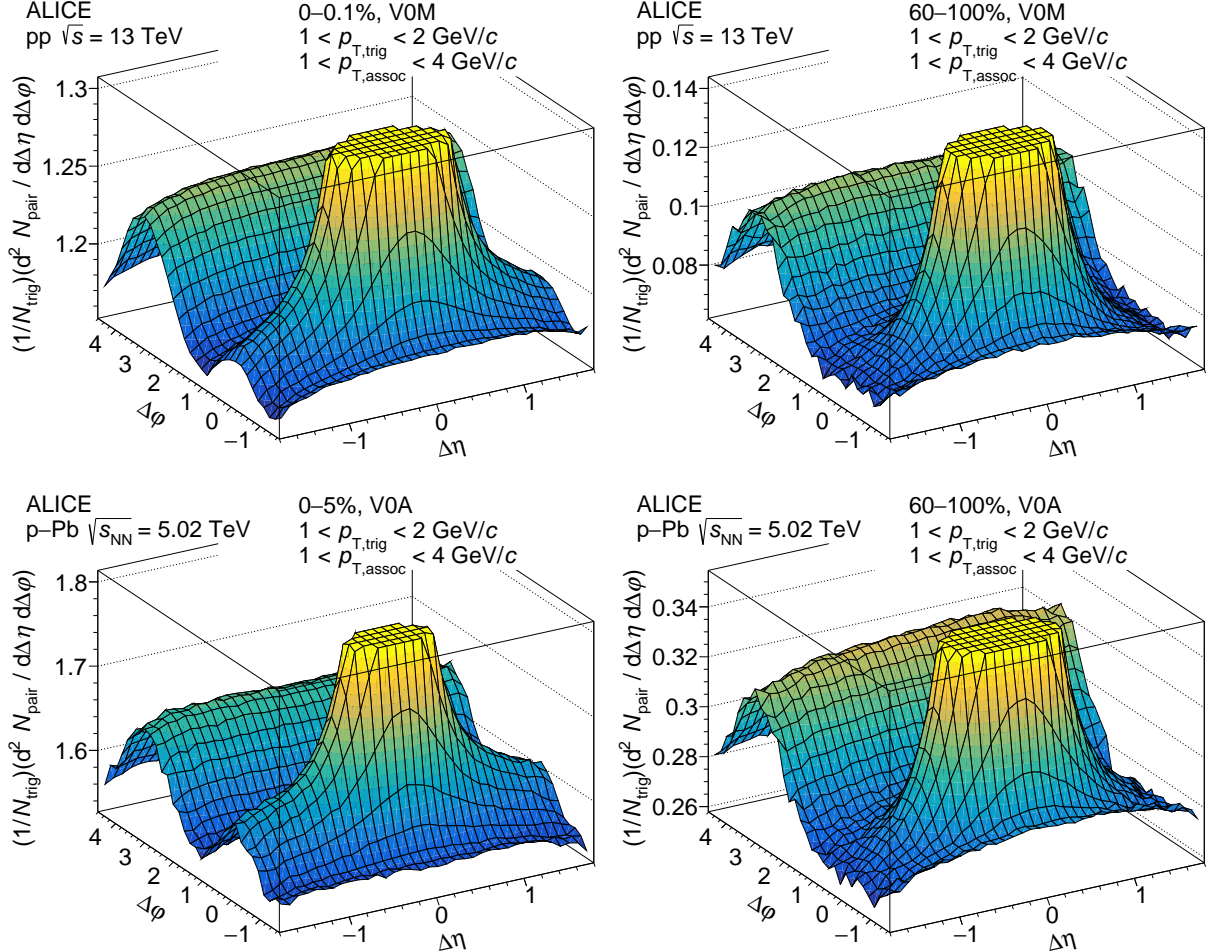


Figure 1: Two-dimensional correlation functions are presented for high-multiplicity (0–0.1% or 0–5%, on the left) and low-multiplicity (60–100%, on the right) events in $\sqrt{s} = 13$ TeV pp collisions in the top panels. The corresponding distributions for $\sqrt{s_{\text{NN}}} = 5.02$ TeV p–Pb collisions are shown in the bottom panels. All correlation functions are shown for $1 < p_{\text{T,trig}} < 2 \text{ GeV}/c$ and $1 < p_{\text{T,assoc}} < 4 \text{ GeV}/c$, respectively.

The fully corrected correlation functions from pp and p–Pb collisions are shown in Fig. 1. The z -axis is scaled in order to exhibit the ridge structures at large $\Delta\eta$ regions. As a result, the jet peaks are sheared off in all figures. The flow modulation structure is clearly observed to emerge in the high-multiplicity collisions for both systems, while it is not seen in the low-multiplicity collisions. The away-side regions are populated mostly by back-to-back jet correlations.

The per-trigger yield is determined by integrating the correlation function at large $\Delta\eta$ ($1.6 < |\Delta\eta| < 1.8$) to remove non-flow contributions from near-side jet fragments. The per-trigger yield as a function of $\Delta\phi$ is expressed as

$$Y(\Delta\varphi) = \frac{1}{N_{\text{trig}}} \frac{dN_{\text{pair}}}{d\Delta\varphi} = \int_{1.6 < |\Delta\eta| < 1.8} \left[\frac{1}{N_{\text{trig}}} \frac{d^2N_{\text{pair}}}{d\Delta\eta d\Delta\varphi} \right] \frac{1}{\delta_{\Delta\eta}} d\Delta\eta, \quad (2)$$

where the factor $\delta_{\Delta\eta} = 0.4$ normalizes the obtained per-trigger yield per unit of pseudorapidity. The per-trigger yields are extracted for the considered $p_{T,\text{trig}}$ and $p_{T,\text{assoc}}$ intervals in several multiplicity classes: 0–0.1%, 1–5%, 5–20%, 20–60%, and 60–100% in pp collisions, and 0–5%, 5–10%, 10–20%, 20–40%, 40–60%, and 60–100% in p–Pb collisions. The conversion of the measured forward event multiplicities to the charge-particle multiplicities N_{ch} at midrapidity ($|\eta| < 0.5$) used in Sec. 5 is based on Ref. [98].

3.2 Extraction of flow coefficients

As discussed in Refs. [10, 19], the correlation function in a given multiplicity interval is fitted with

$$Y_{\text{HM}}(\Delta\varphi) = G (1 + 2v_{2,2} \cos(2\Delta\varphi) + 2v_{3,3} \cos(3\Delta\varphi)) + F Y_{\text{LM}}(\Delta\varphi), \quad (3)$$

where $Y_{\text{LM}}(\Delta\varphi)$ is the measured per-trigger yield from low-multiplicity events. The normalization factor for the first three Fourier terms, which parameterize the long-range, flow-like correlation, is denoted as G . The scale factor F compensates for the increased yield of away-side-jet hadrons in the analyzed multiplicity class relative to the low-multiplicity template that corresponds to the 60–100% class [81, 82]. The fit determines the scale factor F , pedestal G , and $v_{n,n}$ and is performed in various high-multiplicity classes as well as in different $p_{T,\text{trig}}$ intervals. This method assumes that Y_{LM} does not contain a near-side-peak structure that would originate from jet fragmentation or a near-side ridge. Furthermore it is assumed that the shape of the away-side-peak structure remains the same when changing the multiplicity class. The first assumption is ensured using the selected low-multiplicity template which does not have a strong near-side-peak structure compared to the studied higher-multiplicity classes. The second assumption, which involves the modification of jet shapes, was tested by projecting the near-side jet peaks onto $\Delta\eta$. This modification of the jet shape is considered as one of the sources of systematic uncertainty and will be discussed in Sec. 4.

Figure 2 shows the template fit results for the 0–0.1% multiplicity interval in pp collisions at $\sqrt{s} = 13$ TeV. Values of the extracted scale factor F in different multiplicity intervals and systems are summarized in Table 1. In pp collisions, the value of F is observed to increase slightly as the event multiplicity increases. The F value, which is measured for the highest-multiplicity bin, is approximately 25% larger than the value found for the 20–60% bin. A similar dependence on multiplicity is observed for p–Pb collisions, although the dependence on the multiplicity interval is weaker. In the first three columns of Table 1, representing collisions with higher multiplicities, there is an increase in the F value, while as shown by the subsequent columns, there is a decrease for lower multiplicity collisions. When comparing the F values from pp and p–Pb collisions, which have similar centrality, the value of F in p–Pb collisions is found to be smaller and closer to unity. This suggests that the jet fragmentation yield on the away-side increases with multiplicity, and that this feature is more pronounced in pp collisions. The difference between the two systems is likely to be explained by the true-geometry-driven centrality in p–Pb collisions, as opposed to the jet-dominated bias in pp collisions. The previous analyses published by ALICE in Refs. [17, 83] assumed that the jet contribution remains constant as a function of multiplicity (i.e. F was assumed to be 1). However, this assumption may lead to an underestimation of non-flow contamination in the measurements of anisotropic flow.

In the following, the near and away-side jet fragmentation yields are calculated to verify the template fit method by comparing the jet fragmentation yields to the PYTHIA model. The away-side jet fragmentation yields in the PYTHIA model are obtained using the standard $\Delta\varphi$ analysis [106], while in the data, the away-side jet fragmentation yields are extracted using the template fit method because of the flow

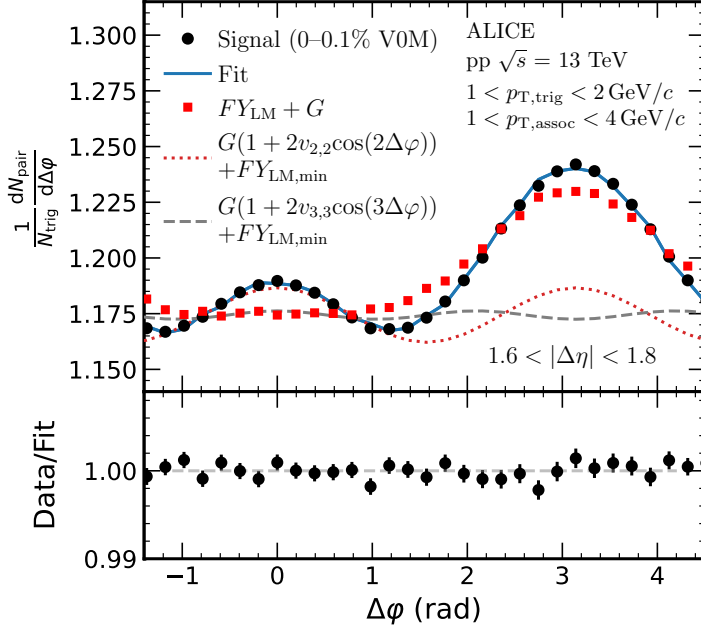


Figure 2: Per-trigger yield in $1.6 < |\Delta\eta| < 1.8$ extracted from 0–0.1% and 60–100% multiplicity percentile events in $\sqrt{s} = 13$ TeV pp collisions. The data are fitted with the template fit method described by Eq. 3. The black markers show the signal for the 0–0.1% multiplicity percentile. The red squares correspond to the low-multiplicity signal. The red and gray curves correspond to the extracted $v_{2,2}$ and $v_{3,3}$ signals, respectively. To improve visibility, the baselines of flow signals are shifted by $FY_{LM,min}$, which represents the minimum yield of $FY_{LM}(\Delta\varphi)$. The signal-to-fit ratio is shown in the bottom panel. The χ^2 divided by the number of degrees of freedom is 0.894.

modulations in the data. The comparison between the data and the PYTHIA model provides a validation of the template fit method.

Equivalently to Eq. (2), measured data are used to obtain the near-side $\Delta\eta$ correlations with

$$Y(\Delta\eta) = \frac{1}{N_{\text{trig}}} \frac{dN_{\text{pair}}}{d\Delta\eta} = \int_{|\Delta\varphi| < 1.3} \left[\frac{1}{N_{\text{trig}}} \frac{d^2N_{\text{pair}}}{d\Delta\eta d\Delta\varphi} \right] \frac{1}{\delta_{\Delta\varphi}} d\Delta\varphi - D_{ZYAM}, \quad (4)$$

where $\delta_{\Delta\varphi} = 2.6$ and D_{ZYAM} defines the baseline of the ZYAM background subtraction [107]. The baseline is obtained by finding the minimum of the distribution defined by the integral in Eq. (4). As flow has a weak η dependence [7, 108, 109], the jet-fragmentation yield can be calculated after the ZYAM background subtraction [107]. The near-side jet-like yields were extracted by integrating the $Y(\Delta\eta)$

$$Y_{\text{frag}}^{\text{near}} = \int_{|\Delta\eta| < 1.3} \left(\frac{1}{N_{\text{trig}}} \frac{dN_{\text{pair}}}{d\Delta\eta} \right) d\Delta\eta. \quad (5)$$

The away-side jet-like yield in data is calculated by integrating the low-multiplicity template over $\pi/2 < \Delta\varphi < 3/2\pi$ and scaling it by the parameter F from Eq. (3), $Y_{\text{frag}}^{\text{away,HM}} = Y_{\text{frag}}^{\text{away,LM}} \times F$. The Y_{frag}

Table 1: The scale factor F for various multiplicity intervals in pp collisions (top) and p–Pb collisions (bottom), with $1 < p_{T,\text{trig}} < 2$ GeV/c and $1 < p_{T,\text{assoc}} < 4$ GeV/c. The table reports statistical uncertainties only. Average systematic uncertainty of F is about 3.8% for both collision systems and multiplicity intervals.

V0M (pp)	0–0.1%	1–5%	5–20%	20–60%		
F	1.504 ± 0.017	1.414 ± 0.030	1.360 ± 0.019	1.208 ± 0.015		
V0A (p–Pb)	0–5%	5–10%	10–20%	0–20%	20–40%	40–60%
F	1.135 ± 0.026	1.140 ± 0.026	1.152 ± 0.021	1.145 ± 0.017	1.092 ± 0.015	1.083 ± 0.015

is directly obtained by integrating the away-side low-multiplicity $\Delta\phi$ correlation function in the low-multiplicity sample over $\pi/2 < \Delta\phi < 3\pi/2$. As PYTHIA does not include any flow contributions in its model, Y^{away} can be directly measured from the $\Delta\phi$ correlation functions.

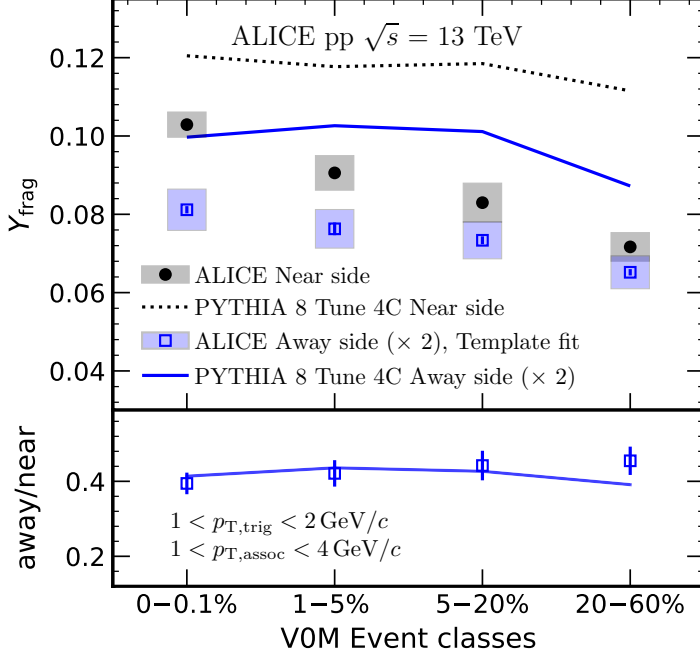


Figure 3: The Y_{frag} for the near- and away-side as a function of multiplicity percentiles with both ALICE and PYTHIA data. Systematic uncertainties are represented by the boxes. The bottom panel presents ratios of the yields. Here the reported uncertainty is obtained by adding statistical error and systematic uncertainty in quadrature. For PYTHIA, the statistical uncertainty is smaller than the thickness of the lines.

Figure 3 presents the $Y_{\text{frag}}^{\text{near}}$ and $Y_{\text{frag}}^{\text{away}}$, for both ALICE data and PYTHIA 8 Tune 4C [110], as a function of the V0M multiplicity intervals in pp collisions at $\sqrt{s} = 13$ TeV. The transverse momentum range for trigger particles is $1 < p_{\text{T,trig}} < 2$ GeV/ c and for associated particles $1 < p_{\text{T,assoc}} < 4$ GeV/ c . The near-to away-side ratio for ALICE and PYTHIA data is shown in the bottom panel. While PYTHIA overestimates both near-side and away-side yields measured by ALICE, the corresponding ratio is consistent with the ALICE data in the all considered V0M multiplicity intervals. The value of this ratio can be explained by the pair acceptance effect caused by the limited ALICE η acceptance [106]. The observed agreement implies that the enhanced jet fragmentation yields in the away-side in high-multiplicity events with respect to low-multiplicity events [81, 82] are taken into account by the low-multiplicity template method. In summary, the difference between the near-side and away-side jet fragmentation yields in PYTHIA is solely caused by the jet acceptance effects which affect the two-particle correlation functions. The corresponding ratio in data, where the away-side jet fragmentation yields are measured with the low-multiplicity template, agrees well with PYTHIA as well as with the expectation in Ref. [106].

The flow coefficients, v_n , of the trigger particles, can be extracted from the template fit with the use of the observed factorization of $v_{n,n}$ coefficients to single harmonics [10, 19] by using

$$v_n(p_{\text{T,trig}}) = v_{n,n}(p_{\text{T,trig}}, p_{\text{T,assoc}}) / \sqrt{v_{n,n}(p_{\text{T,assoc}}, p_{\text{T,assoc}})}, \quad (6)$$

where $v_{n,n}(p_{\text{T,assoc}}, p_{\text{T,assoc}})$ denote $v_{n,n}$ coefficients extracted using trigger and associated particles with p_{T} in the range 1–4 GeV/ c . In the following sections, unless explicitly stated otherwise, v_n will refer to $v_n(p_{\text{T,trig}})$. Different event scale selections were investigated by selecting events that include a hard jet or a high- p_{T} leading particle at midrapidity (i.e., the particle with the highest reconstructed p_{T} inside the

acceptance region in an event). This event scale was set by requiring a minimum p_T of the leading track ($p_{T,\text{LP}}$) or the reconstructed jet ($p_{T,\text{jet}}^{\text{ch}}$) at midrapidity [73]. The leading particle track was required to be within $|\eta| < 0.9$ and $0 < \varphi < 2\pi$, and the jets were reconstructed with the anti- k_T algorithm [111, 112], with $R = 0.4$ using charged particles only. Jet constituents were combined using the boost-invariant p_T recombination scheme. The jets are selected in the full azimuth ($0 < \varphi < 2\pi$) and their pseudorapidity is constrained to $|\eta_{\text{jet}}| < 0.4$. The p_T of jets $p_{T,\text{jet}}^{\text{ch}}$ is corrected for the underlying event density that is measured using the k_T algorithm with $R = 0.2$ following the procedure described in Ref. [113].

4 Systematic uncertainties

Table 2: The relative systematic uncertainties of Y^{near} , $Y^{\text{away,LM}}$, F , v_2 , and v_3 . The quantities Y^{near} , $Y^{\text{away,LM}}$, F are only measured in pp collisions, whereas v_2 and v_3 are measured in both pp and p–Pb collisions. The quoted ranges correspond to minimum and maximum uncertainties. Those uncertainties that are considered to be negligible are marked “negl.”. The systematic variations which are not relevant for the measurement are denoted as “N.A.”.

Sources	Systematic uncertainty (%)											
	Y^{near}			$Y^{\text{away,LM}}$		F			v_2		v_3	
	pp	pp	pp	pp	pp	pp	pp	p–Pb	pp	p–Pb	pp	p–Pb
Primary vertex	± 0.2 – 0.5	± 0.1	± 1.0 – 2.5	± 0.2 – 1.8	± 0.8	± 1.4	± 3.9					
Pileup rejection	± 0.1 – 0.5	± 0.2	± 0.4 – 1.5	negl.	± 0.6	negl.	± 1.4					
Tracking	± 1.0 – 3.0	± 2.0	± 0.6 – 2.4	± 0.2 – 3.0	negl.	± 5.0 – 6.9	negl.					
Event mixing	± 0.2 – 0.7	± 0.2 – 0.5	± 0.0 – 3.3	± 0.3 – 4.6	± 0.8	± 2.8 – 3.1	± 0.8					
Low-mult. definition	N.A.	± 0.5 – 3.5	± 0.7 – 6.0	negl.	± 1.9	negl.	± 9.2					
ITS–TPC matching	± 2.0 – 3.0	± 2.0 – 3.0	N.A.	N.A.	N.A.	N.A.	N.A.	N.A.	N.A.	N.A.	N.A.	N.A.
Efficiency correction	± 1.0 – 4.4	± 1.0 – 4.4	N.A.	N.A.	N.A.	N.A.	N.A.	N.A.	N.A.	N.A.	N.A.	N.A.
$\Delta\eta$ gap range	N.A.	N.A.	± 0.1 – 3.2	± 1.0 – 5.0	± 0.4	negl.	negl.					
Jet shape modification	N.A.	N.A.	N.A.	± 1.0	± 1.0	± 3.0	± 8.0					
Total (in quadrature)	± 2.5 – 6.1	± 5.0 – 5.5	± 1.8 – 7.1	± 1.3 – 5.8	± 2.5	± 6.8 – 8.0	± 12.8					

Systematic uncertainties are estimated by varying the analysis selection criteria and corrections. Independent systematic checks are performed and the differences between results obtained from each variation and the default selection are considered as the systematic uncertainty for each source [114]. The total systematic uncertainty is obtained by adding the contributions from different sources in quadrature. A summary of all systematic uncertainties is provided in Table 2.

The uncertainty attributed to the chosen primary vertex range is estimated by varying the selected range from $|z_{\text{vtx}}| < 8$ cm to $|z_{\text{vtx}}| < 6$ cm. The variation of the range allows testing detector acceptance effects on the measurement.

Another source of systematic uncertainty is related to pileup rejection. The rejection of pileup events is adjusted by modifying the number of track contributors required for the reconstruction of pileup event vertices, changing it from the default value of 3 to 5.

The systematic uncertainty due to the choice of track-selection criteria is estimated by employing alternative track-selection criteria, which single out so-called “global track”, which are described in Ref. [115]. A global track is required to have two hits in the ITS (at least one in the SPD) and at least 70 clusters in the TPC. Due to inefficiencies in certain parts of the SPD, the azimuthal distribution of global tracks is not uniform. This can be corrected by using corresponding mixed events and accounting for the corresponding tracking efficiency.

An additional systematic uncertainty from the event-mixing is estimated by varying the interval of the primary vertex range, where events are mixed. The default size of the primary vertex bins of mixed

events is decreased from 2 cm to 1 cm.

The systematic uncertainty associated with the low-multiplicity definition is estimated by changing the range of the low-VOM-multiplicity interval. There is no universal definition for the low-multiplicity interval. The default range for the low-multiplicity interval in the present article is 60–100%, and it is changed to 70–100% to estimate the related systematic uncertainty. Note that for the measurement of Y^{near} , the low-multiplicity-interval definition is irrelevant.

The systematic uncertainty resulting from matching a track reconstructed by the TPC and the corresponding signal in the ITS is estimated by evaluating the fraction of mismatches in real data using simulations. Primary tracks have a higher matching efficiency than secondary tracks produced far from the interaction point or in interactions with detector material. To address the effect of different fractions of primary and secondary tracks in data and simulations on the matching efficiency, particle abundances in the simulation are reweighted to reflect real data. This resulted in modified matching efficiency.

The systematic uncertainty arising from the efficiency correction is estimated by performing a closure test, where two correlation functions are compared. The first correlation function is constructed using true information from the Monte Carlo samples described in Sec. 2. This provides a baseline for the expected correlation function. The second correlation function is constructed using reconstructed tracks corrected for tracking efficiency. By comparing the two correlation functions, it is possible to estimate the magnitude of the uncertainty introduced by the correction.

Due to the limited η acceptance of the TPC, non-flow contributions, mainly originating from fragmentation of jets, affect the flow measurement. As the shape of short-range correlations, mostly attributed to jets, is getting broader with decreasing p_T , the systematic uncertainty from η acceptance significantly depends on p_T . To estimate the related uncertainty, the long range $\Delta\phi$ correlations are measured for an extended $\Delta\eta$ gap, the default size of $\Delta\eta$ gap 1.6 is increased to 1.7.

Finally, it is worth considering the possible impact of the multiplicity dependence of the jet-shape modifications discussed in Sec. 3. This is studied by examining the shape modification of the jet-peak distribution in the near-side region as a function of $\Delta\eta$ and multiplicity. The observed change in the width is used to estimate the possible effect on the long-range, per-trigger-yield distribution as a function of $\Delta\phi$. The effect on v_2 is found to be less than 1% in pp and p–Pb collisions for the kinematic ranges analyzed. The effect on v_3 is found to be less than 8% in p–Pb collisions. These values are included in the total systematic uncertainty. However, it is important to note that other analyses with different kinematic ranges should also perform a similar check to assess the systematic uncertainty associated with this effect. It is possible that this effect may not always be as small as in our analysis.

5 Results

5.1 Transverse-momentum and multiplicity dependence of anisotropic flow

Figure 4 illustrates the extracted values of v_2 and v_3 as a function of $p_{T,\text{trig}}$ as obtained from Eq. (3). The results correspond to the high-multiplicity pp collisions at $\sqrt{s} = 13$ TeV and p–Pb collisions at $\sqrt{s_{\text{NN}}} = 5.02$ TeV. Both sets of results demonstrate an increasing trend in the magnitudes of v_n with rising $p_{T,\text{trig}}$. The v_2 data points reach a maximum between 2.5 and 3.0 GeV/ c , similarly to what has been observed in Pb–Pb collisions [5, 116]. The magnitudes of v_2 in p–Pb collisions are higher than those in pp collisions, which might be related to the larger p–Pb system size together with a likely longer lifetime of the hypothetically created medium. However, the magnitudes of v_3 are similar in both systems, indicating that v_3 is less sensitive to the size of the systems. These results are comparable to those obtained by ATLAS in different multiplicity classes, where the same method was used to extract the flow coefficients [19]. Even though the $\Delta\eta$ and $p_{T,\text{assoc}}$ ranges used by ATLAS are wider, $2.0 < |\Delta\eta| < 5.0$ and $0.5 < p_{T,\text{assoc}} < 5$ GeV/ c , respectively, the results are consistent within uncertainties.

Figure 5 presents the magnitudes of v_2 and v_3 , as a function of charged-particle multiplicity at midrapidity for both pp collisions at $\sqrt{s} = 13$ TeV and p–Pb collisions at $\sqrt{s_{\text{NN}}} = 5.02$ TeV. As in Fig. 4, the $\Delta\eta$ gap is $1.6 < |\Delta\eta| < 1.8$ and v_2 is measured in $1 < p_{\text{T}} < 4 \text{ GeV}/c$ for both collision systems. Additionally, the corresponding results for pp collisions at $\sqrt{s} = 13$ TeV with $1 < p_{\text{T}} < 2 \text{ GeV}/c$ are presented. First, it is observed that the magnitude of v_n increases with increasing multiplicity for both collision systems and p_{T} -ranges. Second, v_2 in p–Pb is higher than in pp collisions in the measured multiplicity range. These two observations are compatible with previous results from Refs. [10, 11, 19]. There is no significant difference between the two collision systems when considering the v_3 dependence on multiplicity as shown on the right-hand-side panel of Fig. 5. The v_3 measurements exhibit a comparable subtle dependence on multiplicity, with higher values observed in collisions with greater particle multiplicities. For the two different p_{T} intervals presented for the pp collisions, the v_2 in $1.0 < p_{\text{T}} < 4.0 \text{ GeV}/c$ shows a hint of larger magnitude than the v_2 in $1.0 < p_{\text{T}} < 2.0 \text{ GeV}/c$. The difference in magnitude is significant only in the highest multiplicity point. This agrees with what is observed in Fig. 4, where the v_2 magnitude has its largest value in $2.5 < p_{\text{T}} < 3.0 \text{ GeV}/c$. It is found that for the considered p_{T} selections, the observed multiplicity dependencies differ only marginally. It is worth noting that the results presented from pp and p–Pb collisions were obtained from two different beam energies. In Ref. [19], it was found that the magnitudes of v_2 and v_3 in pp collisions between 13 and 5.02 TeV show no significant variation with center-of-mass energy.

5.2 Event-scale dependence of the flow coefficients

Figure 6 presents the extracted magnitude of v_2 and v_3 as a function of the minimum p_{T} of the leading particle ($p_{\text{T},\text{min}}^{\text{LP}}$) and that of the jet ($p_{\text{T},\text{min}}^{\text{jet}}$) as introduced in Sec. 1. The results are presented for the 0–0.1% multiplicity class of pp collisions at $\sqrt{s} = 13$ TeV and for the two different p_{T} -ranges. To reduce the impact of the detector edge effects on the jet measurements, the jet axes are required to have a pseudorapidity $|\eta_{\text{jet}}| < 0.4$, following a similar selection as in Refs. [117–119]. The v_2 and v_3 values for both p_{T} ranges do not show any dependence on event-scale selection within the uncertainties. This finding is consistent with the results of the ridge yields [73] and v_2 measurements with a tagged Z boson from the ATLAS collaboration [120]. These results suggest that the presence of a hard-scattering process does not significantly change the long-range correlation involving soft particles. However, the presented measurements are only limited to the low $p_{\text{T}}^{\text{jet}}$. Future measurements with multi-jet events at midrapidity

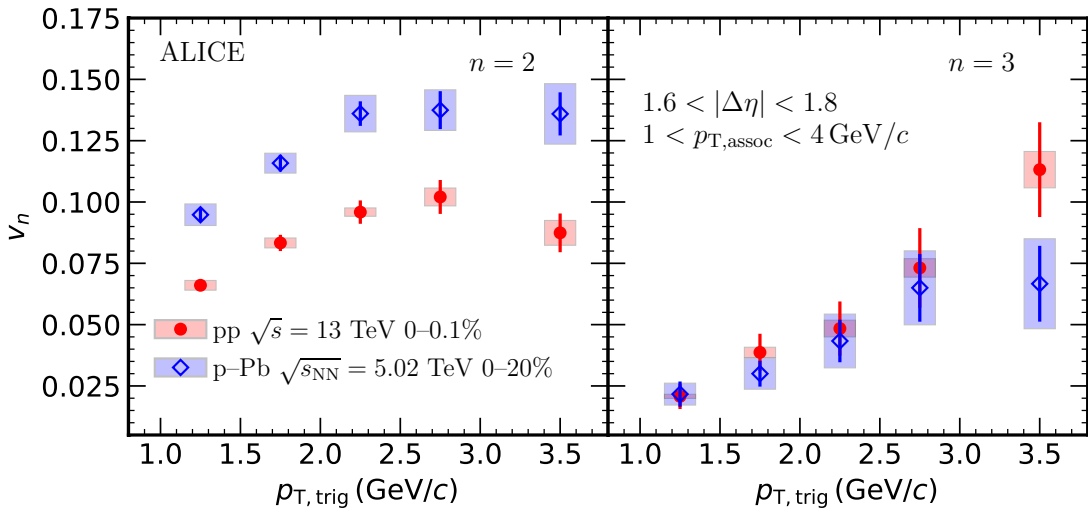


Figure 4: The magnitude of v_2 (left) and v_3 (right) as a function of p_{T} for the 0–0.1% multiplicity interval in pp collisions at $\sqrt{s} = 13$ TeV and 0–20% in p–Pb collisions at $\sqrt{s_{\text{NN}}} = 5.02$ TeV. The boxes around the data points represent the estimated systematic uncertainty and the error bars correspond to statistical errors.

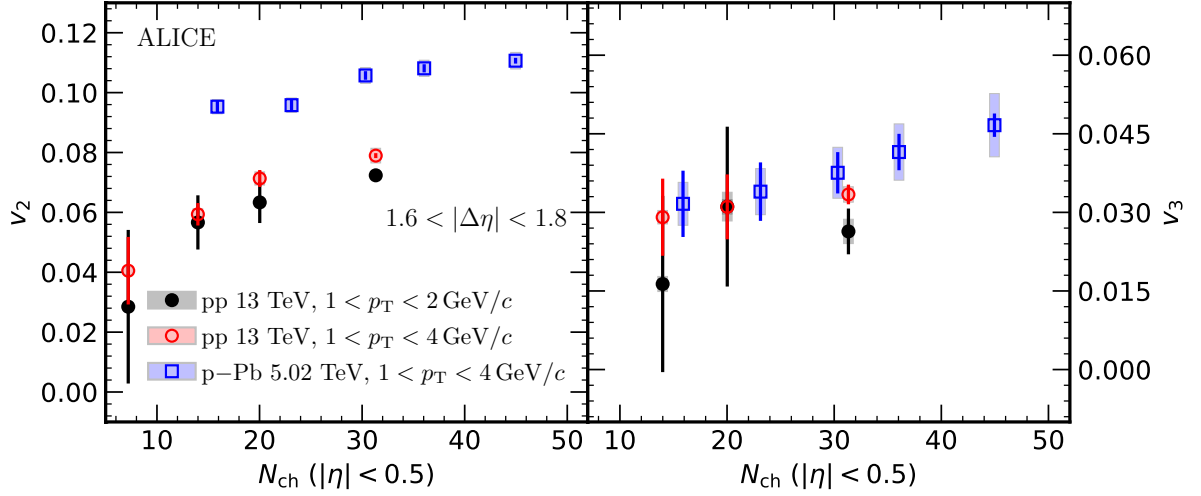


Figure 5: The magnitudes of v_2 (left panel) and v_3 (right panel) for two different collision systems, pp and p–Pb as a function of charged-particle multiplicity at midrapidity. For pp collisions, two different p_T intervals are shown, $1.0 < p_T < 2.0 \text{ GeV}/c$ and $1.0 < p_T < 4.0 \text{ GeV}/c$. The boxes around the data points represent the estimated systematic uncertainties and the error bars corresponds to statistical errors.

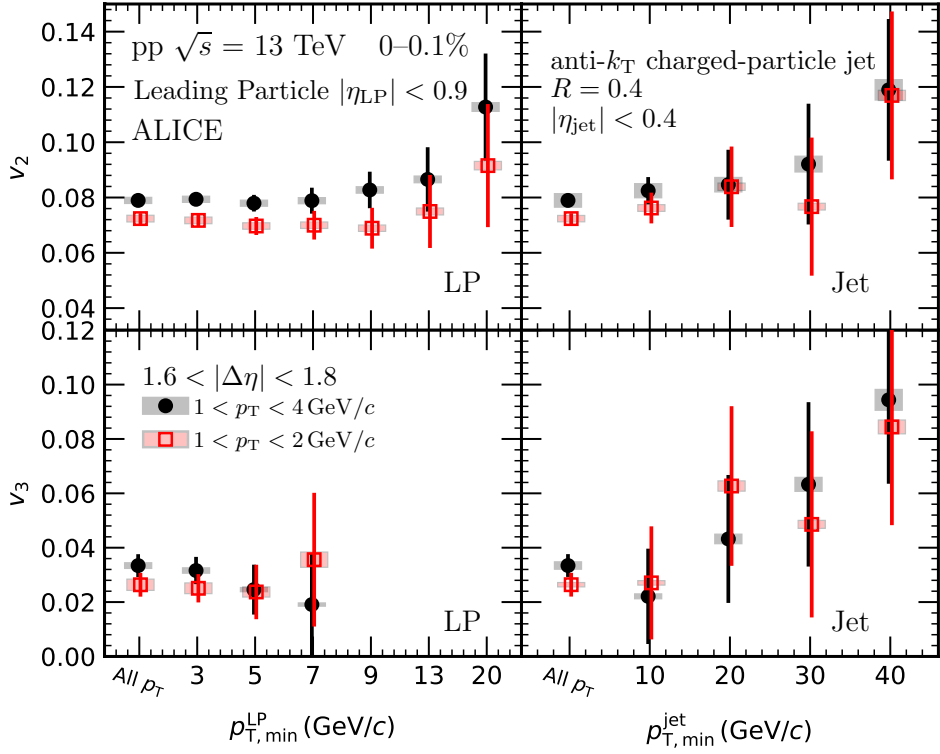


Figure 6: The magnitudes of v_2 (top) and v_3 (bottom) as a function of $p_{T,\text{min}}^{\text{LP}}$ (left) and $p_{T,\text{min}}^{\text{jet}}$ (right) for the high-multiplicity in pp collisions at $\sqrt{s} = 13 \text{ TeV}$. The measured p_T intervals are $1 < p_T < 2 \text{ GeV}/c$ (in red) and $1 < p_T < 4 \text{ GeV}/c$ (in black). The statistical errors and systematic uncertainties are shown as vertical bars and boxes, respectively.

with higher Q^2 reach can shed more light on the expected impact parameter dependence [84–86].

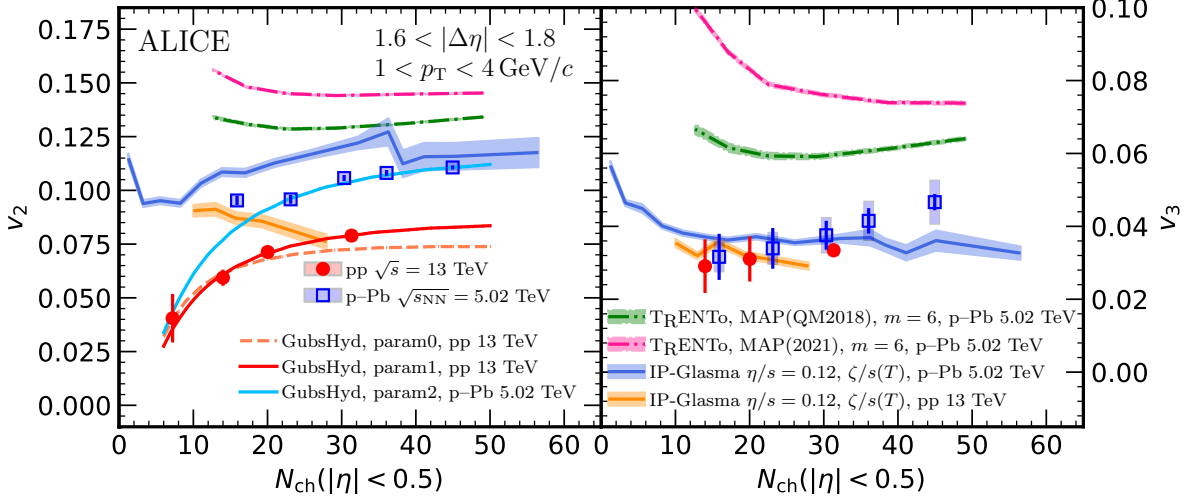


Figure 7: The measured and calculated evolution of v_2 (left) and v_3 (right) in pp and p–Pb collisions as a function of charged-particle multiplicity at midrapidity. The blue and red markers represent the measured p–Pb and pp data, respectively. The calculations provided by hydrodynamical models [52, 55, 64, 74] are presented with colored lines. The corresponding bands mark their statistical uncertainty. For GubsHyd calculations, the statistical uncertainty is smaller than the line thickness.

5.3 Comparisons with models

In this section, the results are compared to various model calculations. The results from p–Pb collisions are compared with hydrodynamic calculations using the parameterization from an improved global Bayesian analysis. The analysis involves new sophisticated collective flow observables as obtained from two different beam energies in Pb–Pb collisions [55], constraining the initial conditions and transport properties of the QGP. This hydrodynamic model, TRENTo+iEBE-VISHNU, consists of the TRENTo model [121] to simulate the initial condition, which is connected with a free streaming to a 2+1 dimensional causal hydrodynamic model VISH2+1 [122]. The evolution is continued after hadronization with a hadronic cascade model (UrQMD) [41, 42]. A model calculation is performed using the best-fit parameterization for transport coefficients selected based on maximum a posteriori (MAP) for Pb–Pb collisions at $\sqrt{s_{\text{NN}}} = 5.02 \text{ TeV}$. Two different MAP values are used for the calculations. They are based on Ref. [55] and Ref. [52] and in Fig. 7 they are labeled MAP(2021) and MAP(QM2018), respectively. The parameterization for the initial conditions, which include a sub-nucleon structure with six constituent partons per nucleon ($m = 6$), is taken from a model calibration with additional p–Pb data [56]. All kinematic selections, such as the transverse momentum and pseudorapidity intervals, are matched to the data reported in this article. The flow coefficients in the hydrodynamic calculation are extracted with the two-particle cumulant method, as the TRENTo+iEBE-VISHNU does not contain any non-flow.

Figure 7 shows that TRENTo+iEBE-VISHNU overestimates both v_2 and v_3 . In the studied range, the v_2 and v_3 data increase with multiplicity. However, TRENTo+iEBE-VISHNU predicts the opposite trend, which is similar to what is found in large collision systems [47]. The large discrepancies in the prediction might be alleviated by inclusion of the newly measured p–Pb constraints in a future Bayesian parameter estimation as well as by improvements of the initial condition model for small-system collisions.

The results are also compared with IP-Glasma+MUSIC+UrQMD hydrodynamic calculations [74]. This model uses IP-Glasma initial conditions [30] including sub-nucleonic fluctuations with three hot spots per nucleon. The hydrodynamic evolution is performed by MUSIC [36] and coupled with UrQMD [41, 42], which performs hadronic cascade. The model calculations are performed assuming constant $\eta/s = 0.12$ and a temperature dependent $\zeta/s(T)$ [123]. This model describes well the multiplicity dependence

of v_2 in p–Pb collisions and the magnitude at the highest multiplicity within the statistical uncertainties of the model but overestimates the data for the lower multiplicity classes. As for pp collisions, the calculations clearly miss both the observed magnitude except for $N_{\text{ch}} > 25$ as well as the trend of the multiplicity dependence. The model shows that v_2 decreases with increasing multiplicity, while the experimental result shows the opposite. For v_3 , the model accurately describes the magnitudes and multiplicity dependence across the measured multiplicity ranges. The magnitudes of v_3 are slightly smaller in pp collisions than in p–Pb collisions according to the calculations, which agrees with the data within the uncertainties. The level of agreement between data and the IP Glasma model calculations is found to be similar to the results reported in Ref. [13].

Finally, the results are compared with the GubsHyd model, a semi-analytical model based on the analytical Gubser solution to hydrodynamic equations [62, 63], known as Gubser flow. In Gubser flow, the initial state of conformal matter is linearly perturbed by an initial elliptic shape. The model is employed to shed light on the possible sources of the observed discrepancy between more realistic models mentioned above and the measurements in pp collisions [64]. Instead of modeling the initial entropy density in this model, as it is typically done in T_RENTo or IP-Glasma, the initial state fluctuation is modeled directly. It assumes that proton ellipticity ε_2 and RMS radius r_{rms} fluctuate independently. These fluctuations are described by Gaussian probability distributions, which have widths σ_ε and σ_r , respectively. The multiplicity dependence of the $v_2\{2\}$ of two-particle correlation functions depends on σ_r and $\chi\sigma_\varepsilon$, where the coefficient χ encapsulates a correction for idealizations used in GubsHyd, including the absence of dissipation effects. The values of σ_r and $\chi\sigma_\varepsilon$ were obtained by comparing the model with data. Since no non-flow effect is considered in the calculation, $v_2\{2\}$ is comparable with the flow measurements in the present study. The calculations for two sets of parameters are compared to data in Fig. 7. The “param0” parameterization is based on the prediction proposed in Ref. [64] that $\chi\sigma_\varepsilon = 0.097$ and $\sigma_r = 0.4$ fm. The other parameterizations “param1” and “param2” employ different $\chi\sigma_\varepsilon$ and σ_r values. The model captures the multiplicity dependence of v_2 well.

In summary, the measured v_2 value decrease with decreasing multiplicity in both pp and p–Pb collisions. This trend is also predicted by GubsHyd model calculations (Refs. [64] and [124]). Interestingly, the opposite trend is observed for the IP-GLASMA+MUSIC+UrQMD hydrodynamic calculations of v_2 , where the value decreases with increasing charged-particle multiplicity [74]. Approaching a lower bound for the size of a hydrodynamized system as predicted in Ref. [64], the decreasing trend of v_2 , obtained by lowering the charged-particle multiplicity, changes and turns out to raise again after the observed minimum. However, this change in multiplicity dependence of v_2 at low multiplicities is still challenging to test with the current experimental uncertainties. For v_3 , the IP-Glasma+MUSIC+UrQMD hydrodynamic calculations [74] are the only ones that accurately describe its magnitude and multiplicity dependence across the measured ranges. The calculations predict that the magnitudes of v_3 are slightly smaller in pp collisions than in p–Pb collisions, within the measured multiplicity ranges. The discrepancies between the predictions and the data can be further studied by including these measurements in a future Bayesian parameter estimation, as well as by improving the initial-condition model for the small-system collisions.

6 Conclusions

Long-range angular correlations for pairs of charged particles are studied in pp collisions at $\sqrt{s} = 13$ TeV and p–Pb collisions at $\sqrt{s_{\text{NN}}} = 5.02$ TeV. Flow coefficients are extracted from long-range correlations ($1.6 < |\Delta\eta| < 1.8$) for a broad range of charged-particle-multiplicity classes using the template method, which allows one to subtract the enhanced away-side jet fragmentation yields in high-multiplicity events with respect to low-multiplicity events. The method that was used to measure the flow coefficients within the considered kinematic ranges has been verified to be stable. The systematic uncertainties on v_2 and v_3 measurements, which reflect the possible differences in the away-side jet peak shapes in

high- and low-multiplicity events, were found to be 1% and 3–8%, respectively. However, it is important that these systematic uncertainties are reevaluated, when analyzing different kinematic ranges, as the effect may not always be negligible. The measured p_T dependence of v_2 and v_3 is consistent with the measurements by ATLAS and shows that both v_2 and v_3 increase with p_T and reach their maximum at $2.5 < p_T < 3.0 \text{ GeV}/c$. The measurement of v_2 as a function of charged-particle multiplicity in $|\eta| < 0.5$ shows a weak multiplicity dependence both for pp and p–Pb collisions and tends to decrease toward lower multiplicities. The pp data suggests that the v_2 signal may disappear when the measurement is pursued further below $N_{\text{ch}} = 10$.

The comparisons to viscous hydrodynamic models show that the magnitudes of v_2 and their multiplicity dependence are not described by state-of-the-art hydrodynamic calculations, which simulated initial conditions with two initial state models, especially for low-multiplicity p–Pb and pp collisions. As initial state effects tend to be more important at low multiplicity [56, 59], these results may help to constrain the modeling of the initial state. Furthermore, the events including hard probes such as jets or high- p_T leading particles do not show any changes both in v_2 and v_3 within the uncertainties, which implies that the long-range correlation of soft particles is not significantly modified by the presence of the hard-scattering process. Even though it would be interesting to compare these results to the EPOS LHC [125] and PYTHIA8 String Shoving models [71, 72] as done in Ref. [17] for the ridge yields, it is not possible to reliably extract the flow coefficients because these models exhibit a near-side ridge structure in low-multiplicity events, thus making the use of the low-multiplicity template ill defined [126].

Acknowledgements

The ALICE Collaboration would like to thank all its engineers and technicians for their invaluable contributions to the construction of the experiment and the CERN accelerator teams for the outstanding performance of the LHC complex. The ALICE Collaboration gratefully acknowledges the resources and support provided by all Grid centres and the Worldwide LHC Computing Grid (WLCG) collaboration. The ALICE Collaboration acknowledges the following funding agencies for their support in building and running the ALICE detector: A. I. Alikhanyan National Science Laboratory (Yerevan Physics Institute) Foundation (ANSL), State Committee of Science and World Federation of Scientists (WFS), Armenia; Austrian Academy of Sciences, Austrian Science Fund (FWF): [M 2467-N36] and Nationalstiftung für Forschung, Technologie und Entwicklung, Austria; Ministry of Communications and High Technologies, National Nuclear Research Center, Azerbaijan; Conselho Nacional de Desenvolvimento Científico e Tecnológico (CNPq), Financiadora de Estudos e Projetos (Finep), Fundação de Amparo à Pesquisa do Estado de São Paulo (FAPESP) and Universidade Federal do Rio Grande do Sul (UFRGS), Brazil; Bulgarian Ministry of Education and Science, within the National Roadmap for Research Infrastructures 2020-2027 (object CERN), Bulgaria; Ministry of Education of China (MOEC) , Ministry of Science & Technology of China (MSTC) and National Natural Science Foundation of China (NSFC), China; Ministry of Science and Education and Croatian Science Foundation, Croatia; Centro de Aplicaciones Tecnológicas y Desarrollo Nuclear (CEADEN), Cubaenergía, Cuba; Ministry of Education, Youth and Sports of the Czech Republic, Czech Republic; The Danish Council for Independent Research | Natural Sciences, the VILLUM FONDEN and Danish National Research Foundation (DNRF), Denmark; Helsinki Institute of Physics (HIP), Finland; Commissariat à l’Energie Atomique (CEA) and Institut National de Physique Nucléaire et de Physique des Particules (IN2P3) and Centre National de la Recherche Scientifique (CNRS), France; Bundesministerium für Bildung und Forschung (BMBF) and GSI Helmholtzzentrum für Schwerionenforschung GmbH, Germany; General Secretariat for Research and Technology, Ministry of Education, Research and Religions, Greece; National Research, Development and Innovation Office, Hungary; Department of Atomic Energy Government of India (DAE), Department of Science and Technology, Government of India (DST), University Grants Commission, Government of India (UGC) and Council of Scientific and Industrial Research (CSIR), India; National

Research and Innovation Agency - BRIN, Indonesia; Istituto Nazionale di Fisica Nucleare (INFN), Italy; Japanese Ministry of Education, Culture, Sports, Science and Technology (MEXT) and Japan Society for the Promotion of Science (JSPS) KAKENHI, Japan; Consejo Nacional de Ciencia (CONACYT) y Tecnología, through Fondo de Cooperación Internacional en Ciencia y Tecnología (FONCICYT) and Dirección General de Asuntos del Personal Académico (DGAPA), Mexico; Nederlandse Organisatie voor Wetenschappelijk Onderzoek (NWO), Netherlands; The Research Council of Norway, Norway; Commission on Science and Technology for Sustainable Development in the South (COMSATS), Pakistan; Pontificia Universidad Católica del Perú, Peru; Ministry of Education and Science, National Science Centre and WUT ID-UB, Poland; Korea Institute of Science and Technology Information and National Research Foundation of Korea (NRF), Republic of Korea; Ministry of Education and Scientific Research, Institute of Atomic Physics, Ministry of Research and Innovation and Institute of Atomic Physics and University Politehnica of Bucharest, Romania; Ministry of Education, Science, Research and Sport of the Slovak Republic, Slovakia; National Research Foundation of South Africa, South Africa; Swedish Research Council (VR) and Knut & Alice Wallenberg Foundation (KAW), Sweden; European Organization for Nuclear Research, Switzerland; Suranaree University of Technology (SUT), National Science and Technology Development Agency (NSTDA) and National Science, Research and Innovation Fund (NSRF via PMU-B B05F650021), Thailand; Turkish Energy, Nuclear and Mineral Research Agency (TENMAK), Turkey; National Academy of Sciences of Ukraine, Ukraine; Science and Technology Facilities Council (STFC), United Kingdom; National Science Foundation of the United States of America (NSF) and United States Department of Energy, Office of Nuclear Physics (DOE NP), United States of America. In addition, individual groups or members have received support from: European Research Council, Strong 2020 - Horizon 2020 (grant nos. 950692, 824093), European Union; Academy of Finland (Center of Excellence in Quark Matter) (grant nos. 346327, 346328), Finland.

References

- [1] **STAR** Collaboration, J. Adams *et al.*, “Experimental and theoretical challenges in the search for the quark gluon plasma: The STAR Collaboration’s critical assessment of the evidence from RHIC collisions”, *Nucl. Phys.* **A757** (2005) 102–183, arXiv:nucl-ex/0501009 [nucl-ex].
- [2] **PHENIX** Collaboration, K. Adcox *et al.*, “Formation of dense partonic matter in relativistic nucleus-nucleus collisions at RHIC: Experimental evaluation by the PHENIX collaboration”, *Nucl. Phys.* **A757** (2005) 184–283, arXiv:nucl-ex/0410003 [nucl-ex].
- [3] **BRAHMS** Collaboration, I. Arsene *et al.*, “Quark gluon plasma and color glass condensate at RHIC? The Perspective from the BRAHMS experiment”, *Nucl. Phys.* **A757** (2005) 1–27, arXiv:nucl-ex/0410020 [nucl-ex].
- [4] **PHOBOS** Collaboration, B. B. Back *et al.*, “The PHOBOS perspective on discoveries at RHIC”, *Nucl. Phys.* **A757** (2005) 28–101, arXiv:nucl-ex/0410022 [nucl-ex].
- [5] **ALICE** Collaboration, B. Abelev *et al.*, “Anisotropic flow of charged hadrons, pions and (anti-)protons measured at high transverse momentum in Pb–Pb collisions at $\sqrt{s_{\text{NN}}} = 2.76 \text{ TeV}$ ”, *Phys. Lett.* **B719** (2013) 18–28, arXiv:1205.5761 [nucl-ex].
- [6] **ALICE** Collaboration, B. Abelev *et al.*, “Elliptic flow of identified hadrons in Pb–Pb collisions at $\sqrt{s_{\text{NN}}} = 2.76 \text{ TeV}$ ”, *JHEP* **06** (2015) 190, arXiv:1405.4632 [nucl-ex].
- [7] **ATLAS** Collaboration, G. Aad *et al.*, “Measurement of the pseudorapidity and transverse momentum dependence of the elliptic flow of charged particles in lead-lead collisions at $\sqrt{s_{\text{NN}}} = 2.76 \text{ TeV}$ with the ATLAS detector”, *Phys. Lett. B* **707** (2012) 330–348, arXiv:1108.6018 [hep-ex].

- [8] **ALICE** Collaboration, “The ALICE experiment – A journey through QCD”, arXiv:2211.04384 [nucl-ex].
- [9] J.-Y. Ollitrault, “Anisotropy as a signature of transverse collective flow”, *Phys. Rev. D* **46** (1992) 229–245.
- [10] **ATLAS** Collaboration, G. Aad *et al.*, “Observation of Long-Range Elliptic Azimuthal Anisotropies in $\sqrt{s}=13$ and 2.76 TeV pp Collisions with the ATLAS Detector”, *Phys. Rev. Lett.* **116** (2016) 172301, arXiv:1509.04776 [hep-ex].
- [11] **CMS** Collaboration, V. Khachatryan *et al.*, “Measurement of long-range near-side two-particle angular correlations in pp collisions at $\sqrt{s}=13$ TeV”, *Phys. Rev. Lett.* **116** (2016) 172302, arXiv:1510.03068 [nucl-ex].
- [12] **CMS** Collaboration, V. Khachatryan *et al.*, “Evidence for collectivity in pp collisions at the LHC”, *Phys. Lett. B* **765** (2017) 193–220, arXiv:1606.06198 [nucl-ex].
- [13] **ALICE** Collaboration, S. Acharya *et al.*, “Investigations of Anisotropic Flow Using Multiparticle Azimuthal Correlations in pp , p – Pb , Xe – Xe , and Pb – Pb Collisions at the LHC”, *Phys. Rev. Lett.* **123** (2019) 142301, arXiv:1903.01790 [nucl-ex].
- [14] **ATLAS** Collaboration, M. Aaboud *et al.*, “Measurement of long-range multiparticle azimuthal correlations with the subevent cumulant method in pp and p + Pb collisions with the ATLAS detector at the CERN Large Hadron Collider”, *Phys. Rev. C* **97** (2018) 024904, arXiv:1708.03559 [hep-ex].
- [15] **CMS** Collaboration, V. Khachatryan *et al.*, “Observation of Long-Range Near-Side Angular Correlations in Proton-Proton Collisions at the LHC”, *JHEP* **09** (2010) 091, arXiv:1009.4122 [hep-ex].
- [16] **LHCb** Collaboration, R. Aaij *et al.*, “Measurements of long-range near-side angular correlations in $\sqrt{s_{NN}}=5$ TeV proton-lead collisions in the forward region”, *Phys. Lett. B* **762** (2016) 473–483, arXiv:1512.00439 [nucl-ex].
- [17] **ALICE** Collaboration, B. Abelev *et al.*, “Long-range angular correlations on the near and away side in p - Pb collisions at $\sqrt{s_{NN}}=5.02$ TeV”, *Phys. Lett. B* **719** (2013) 29–41, arXiv:1212.2001 [nucl-ex].
- [18] **ATLAS** Collaboration, G. Aad *et al.*, “Measurement of long-range pseudorapidity correlations and azimuthal harmonics in $\sqrt{s_{NN}}=5.02$ TeV proton-lead collisions with the ATLAS detector”, *Phys. Rev. C* **90** (2014) 044906, arXiv:1409.1792 [hep-ex].
- [19] **ATLAS** Collaboration, M. Aaboud *et al.*, “Measurements of long-range azimuthal anisotropies and associated Fourier coefficients for pp collisions at $\sqrt{s}=5.02$ and 13 TeV and p + Pb collisions at $\sqrt{s_{NN}}=5.02$ TeV with the ATLAS detector”, *Phys. Rev. C* **96** (2017) 024908, arXiv:1609.06213 [nucl-ex].
- [20] **CMS** Collaboration, V. Khachatryan *et al.*, “Pseudorapidity dependence of long-range two-particle correlations in p Pb collisions at $\sqrt{s_{NN}}=5.02$ TeV”, *Phys. Rev. C* **96** (2017) 014915, arXiv:1604.05347 [nucl-ex].
- [21] **PHENIX** Collaboration, C. Aidala *et al.*, “Creation of quark–gluon plasma droplets with three distinct geometries”, *Nature Phys.* **15** (2019) 214–220, arXiv:1805.02973 [nucl-ex].

- [22] **PHENIX** Collaboration, C. Aidala *et al.*, “Measurements of Multiparticle Correlations in $d + \text{Au}$ Collisions at 200, 62.4, 39, and 19.6 GeV and $p + \text{Au}$ Collisions at 200 GeV and Implications for Collective Behavior”, *Phys. Rev. Lett.* **120** (2018) 062302, arXiv:1707.06108 [nucl-ex].
- [23] M. Gyulassy and M. Plumer, “Jet Quenching in Dense Matter”, *Phys. Lett. B* **243** (1990) 432–438.
- [24] X.-N. Wang and M. Gyulassy, “Gluon shadowing and jet quenching in A + A collisions at $\sqrt{s_{\text{NN}}} = 200$ GeV”, *Phys. Rev. Lett.* **68** (1992) 1480–1483.
- [25] **ALICE** Collaboration, J. Adam *et al.*, “Centrality dependence of particle production in p–Pb collisions at $\sqrt{s_{\text{NN}}} = 5.02$ TeV”, *Phys. Rev. C* **91** (2015) 064905, arXiv:1412.6828 [nucl-ex].
- [26] **CMS** Collaboration, V. Khachatryan *et al.*, “Charged-particle nuclear modification factors in Pb–Pb and p–Pb collisions at $\sqrt{s_{\text{NN}}} = 5.02$ TeV”, *JHEP* **04** (2017) 039, arXiv:1611.01664 [nucl-ex].
- [27] **ALICE** Collaboration, J. Adam *et al.*, “Centrality dependence of charged jet production in p–Pb collisions at $\sqrt{s_{\text{NN}}} = 5.02$ TeV”, *Eur. Phys. J. C* **76** (2016) 271, arXiv:1603.03402 [nucl-ex].
- [28] **ALICE** Collaboration, J. Adam *et al.*, “Multiplicity dependence of charged pion, kaon, and (anti)proton production at large transverse momentum in p–Pb collisions at $\sqrt{s_{\text{NN}}} = 5.02$ TeV”, *Phys. Lett. B* **760** (2016) 720–735, arXiv:1601.03658 [nucl-ex].
- [29] **ALICE** Collaboration, S. Acharya *et al.*, “Constraints on jet quenching in p–Pb collisions at $\sqrt{s_{\text{NN}}} = 5.02$ TeV measured by the event-activity dependence of semi-inclusive hadron-jet distributions”, *Phys. Lett. B* **783** (2018) 95–113, arXiv:1712.05603 [nucl-ex].
- [30] B. Schenke, P. Tribedy, and R. Venugopalan, “Fluctuating Glasma initial conditions and flow in heavy ion collisions”, *Phys. Rev. Lett.* **108** (2012) 252301, arXiv:1202.6646 [nucl-th].
- [31] B. Schenke, P. Tribedy, and R. Venugopalan, “Event-by-event gluon multiplicity, energy density, and eccentricities in ultrarelativistic heavy-ion collisions”, *Phys. Rev. C* **86** (2012) 034908, arXiv:1206.6805 [hep-ph].
- [32] P. F. Kolb and U. W. Heinz, “Hydrodynamic description of ultrarelativistic heavy ion collisions”, arXiv:nucl-th/0305084.
- [33] H. Song and U. W. Heinz, “Causal viscous hydrodynamics in 2+1 dimensions for relativistic heavy-ion collisions”, *Phys. Rev. C* **77** (2008) 064901, arXiv:0712.3715 [nucl-th].
- [34] K. Dusling and D. Teaney, “Simulating elliptic flow with viscous hydrodynamics”, *Phys. Rev. C* **77** (2008) 034905, arXiv:0710.5932 [nucl-th].
- [35] H. Holopainen, H. Niemi, and K. J. Eskola, “Event-by-event hydrodynamics and elliptic flow from fluctuating initial state”, *Phys. Rev. C* **83** (2011) 034901, arXiv:1007.0368 [hep-ph].
- [36] B. Schenke, S. Jeon, and C. Gale, “Elliptic and triangular flow in event-by-event (3+1)D viscous hydrodynamics”, *Phys. Rev. Lett.* **106** (2011) 042301, arXiv:1009.3244 [hep-ph].
- [37] P. Romatschke and U. Romatschke, “Viscosity Information from Relativistic Nuclear Collisions: How Perfect is the Fluid Observed at RHIC?”, *Phys. Rev. Lett.* **99** (2007) 172301, arXiv:0706.1522 [nucl-th].

- [38] H. Niemi, K. Eskola, and R. Paatelainen, “Event-by-event fluctuations in a perturbative QCD + saturation + hydrodynamics model: Determining QCD matter shear viscosity in ultrarelativistic heavy-ion collisions”, *Phys. Rev. C* **93** (2016) 024907, arXiv:1505.02677 [hep-ph].
- [39] S. Jeon and U. Heinz, “Introduction to Hydrodynamics”, *Int. J. Mod. Phys. E* **24** (2015) 1530010, arXiv:1503.03931 [hep-ph].
- [40] P. Romatschke and U. Romatschke, *Relativistic Fluid Dynamics In and Out of Equilibrium*. Cambridge Monographs on Mathematical Physics. Cambridge University Press, 5, 2019. arXiv:1712.05815 [nucl-th].
- [41] S. Bass *et al.*, “Microscopic models for ultrarelativistic heavy ion collisions”, *Prog. Part. Nucl. Phys.* **41** (1998) 255–369, arXiv:nucl-th/9803035.
- [42] M. Bleicher *et al.*, “Relativistic hadron-hadron collisions in the ultrarelativistic quantum molecular dynamics model”, *J. Phys. G* **25** (1999) 1859–1896, arXiv:hep-ph/9909407.
- [43] J. Weil *et al.*, “Particle production and equilibrium properties within a new hadron transport approach for heavy-ion collisions”, *Phys. Rev. C* **94** (2016) 054905, arXiv:1606.06642 [nucl-th].
- [44] ALICE Collaboration, J. Adam *et al.*, “Correlated event-by-event fluctuations of flow harmonics in Pb–Pb collisions at $\sqrt{s_{\text{NN}}} = 2.76 \text{ TeV}$ ”, *Phys. Rev. Lett.* **117** (2016) 182301, arXiv:1604.07663 [nucl-ex].
- [45] ALICE Collaboration, S. Acharya *et al.*, “Systematic studies of correlations between different order flow harmonics in Pb–Pb collisions at $\sqrt{s_{\text{NN}}} = 2.76 \text{ TeV}$ ”, *Phys. Rev. C* **97** (2018) 024906, arXiv:1709.01127 [nucl-ex].
- [46] ALICE Collaboration, S. Acharya *et al.*, “Linear and non-linear flow modes in Pb–Pb collisions at $\sqrt{s_{\text{NN}}} = 2.76 \text{ TeV}$ ”, *Phys. Lett. B* **773** (2017) 68–80, arXiv:1705.04377 [nucl-ex].
- [47] ALICE Collaboration, S. Acharya *et al.*, “Higher harmonic non-linear flow modes of charged hadrons in Pb–Pb collisions at $\sqrt{s_{\text{NN}}} = 5.02 \text{ TeV}$ ”, *JHEP* **05** (2020) 085, arXiv:2002.00633 [nucl-ex].
- [48] ALICE Collaboration, S. Acharya *et al.*, “Multiharmonic Correlations of Different Flow Amplitudes in Pb–Pb Collisions at $\sqrt{s_{\text{NN}}} = 2.76 \text{ TeV}$ ”, *Phys. Rev. Lett.* **127** (2021) 092302, arXiv:2101.02579 [nucl-ex].
- [49] ALICE Collaboration, S. Acharya *et al.*, “Measurements of mixed harmonic cumulants in Pb–Pb collisions at $\sqrt{s_{\text{NN}}} = 5.02 \text{ TeV}$ ”, *Phys. Lett. B* **818** (2021) 136354, arXiv:2102.12180 [nucl-ex].
- [50] ALICE Collaboration, B. Abelev *et al.*, “Centrality dependence of π , K, p production in Pb–Pb collisions at $\sqrt{s_{\text{NN}}} = 2.76 \text{ TeV}$ ”, *Phys. Rev. C* **88** (2013) 044910, arXiv:1303.0737 [hep-ex].
- [51] ALICE Collaboration, K. Aamodt *et al.*, “Higher harmonic anisotropic flow measurements of charged particles in Pb–Pb collisions at $\sqrt{s_{\text{NN}}} = 2.76 \text{ TeV}$ ”, *Phys. Rev. Lett.* **107** (2011) 032301, arXiv:1105.3865 [nucl-ex].
- [52] J. E. Bernhard, J. S. Moreland, S. A. Bass, J. Liu, and U. Heinz, “Applying Bayesian parameter estimation to relativistic heavy-ion collisions: simultaneous characterization of the initial state and quark-gluon plasma medium”, *Phys. Rev. C* **94** (2016) 024907, arXiv:1605.03954 [nucl-th].

- [53] J. E. Bernhard, J. S. Moreland, and S. A. Bass, “Bayesian estimation of the specific shear and bulk viscosity of quark–gluon plasma”, *Nature Phys.* **15** (2019) 1113–1117.
- [54] J. E. Parkkila, A. Onnerstad, and D. J. Kim, “Bayesian estimation of the specific shear and bulk viscosity of the quark-gluon plasma with additional flow harmonic observables”, *Phys. Rev. C* **104** (2021) 054904, arXiv:2106.05019 [hep-ph].
- [55] J. E. Parkkila, A. Onnerstad, S. F. Taghavi, C. Mordasini, A. Bilandzic, M. Virta, and D. J. Kim, “New constraints for QCD matter from improved Bayesian parameter estimation in heavy-ion collisions at LHC”, *Phys. Lett. B* **835** (2022) 137485, arXiv:2111.08145 [hep-ph].
- [56] J. S. Moreland, J. E. Bernhard, and S. A. Bass, “Bayesian calibration of a hybrid nuclear collision model using p–Pb and Pb–Pb data at energies available at the CERN Large Hadron Collider”, *Phys. Rev. C* **101** (2020) 024911, arXiv:1808.02106 [nucl-th].
- [57] K. Dusling and R. Venugopalan, “Evidence for BFKL and saturation dynamics from dihadron spectra at the LHC”, *Phys. Rev. D* **87** (2013) 051502, arXiv:1210.3890 [hep-ph].
- [58] A. Bzdak, B. Schenke, P. Tribedy, and R. Venugopalan, “Initial state geometry and the role of hydrodynamics in proton-proton, proton-nucleus and deuteron-nucleus collisions”, *Phys. Rev. C* **87** (2013) 064906, arXiv:1304.3403 [nucl-th].
- [59] M. Greif, C. Greiner, B. Schenke, S. Schlichting, and Z. Xu, “Importance of initial and final state effects for azimuthal correlations in p+Pb collisions”, *Phys. Rev. D* **96** (2017) 091504, arXiv:1708.02076 [hep-ph].
- [60] H. Mantysaari, B. Schenke, C. Shen, and P. Tribedy, “Imprints of fluctuating proton shapes on flow in proton-lead collisions at the LHC”, *Phys. Lett. B* **772** (2017) 681–686, arXiv:1705.03177 [nucl-th].
- [61] W. Zhao, Y. Zhou, H. Xu, W. Deng, and H. Song, “Hydrodynamic collectivity in proton–proton collisions at 13 TeV”, *Phys. Lett. B* **780** (2018) 495–500, arXiv:1801.00271 [nucl-th].
- [62] S. S. Gubser, “Symmetry constraints on generalizations of Bjorken flow”, *Phys. Rev. D* **82** (2010) 085027, arXiv:1006.0006 [hep-th].
- [63] S. S. Gubser and A. Yarom, “Conformal hydrodynamics in Minkowski and de Sitter spacetimes”, *Nucl. Phys. B* **846** (2011) 469–511, arXiv:1012.1314 [hep-th].
- [64] S. F. Taghavi, “Smallest QCD droplet and multiparticle correlations in p-p collisions”, *Phys. Rev. C* **104** (2021) 054906, arXiv:1907.12140 [nucl-th].
- [65] Z.-W. Lin, C. M. Ko, B.-A. Li, B. Zhang, and S. Pal, “A Multi-phase transport model for relativistic heavy ion collisions”, *Phys. Rev. C* **72** (2005) 064901, arXiv:nucl-th/0411110.
- [66] J. D. Orjuela Koop, A. Adare, D. McGlinchey, and J. L. Nagle, “Azimuthal anisotropy relative to the participant plane from a multiphase transport model in central p + Au , d + Au , and $^3\text{He} + \text{Au}$ collisions at $\sqrt{s_{\text{NN}}} = 200 \text{ GeV}$ ”, *Phys. Rev. C* **92** (2015) 054903, arXiv:1501.06880 [nucl-ex].
- [67] K. Gallmeister, H. Niemi, C. Greiner, and D. H. Rischke, “Exploring the applicability of dissipative fluid dynamics to small systems by comparison to the Boltzmann equation”, *Phys. Rev. C* **98** (2018) 024912, arXiv:1804.09512 [nucl-th].
- [68] A. Kurkela, U. A. Wiedemann, and B. Wu, “Flow in AA and pA as an interplay of fluid-like and non-fluid like excitations”, *Eur. Phys. J. C* **79** (2019) 965, arXiv:1905.05139 [hep-ph].

- [69] A. Kurkela, S. F. Taghavi, U. A. Wiedemann, and B. Wu, “Hydrodynamization in systems with detailed transverse profiles”, *Phys. Lett. B* **811** (2020) 135901, arXiv:2007.06851 [hep-ph].
- [70] V. E. Ambrus, S. Schlichting, and C. Werthmann, “Development of transverse flow at small and large opacities in conformal kinetic theory”, *Phys. Rev. D* **105** (2022) 014031, arXiv:2109.03290 [hep-ph].
- [71] C. Bierlich, G. Gustafson, and L. Lönnblad, “Collectivity without plasma in hadronic collisions”, *Phys. Lett. B* **779** (2018) 58–63, arXiv:1710.09725 [hep-ph].
- [72] C. Bierlich, “Soft modifications to jet fragmentation in high energy proton–proton collisions”, *Phys. Lett. B* **795** (2019) 194–199, arXiv:1901.07447 [hep-ph].
- [73] **ALICE** Collaboration, S. Acharya *et al.*, “Long- and short-range correlations and their event-scale dependence in high-multiplicity pp collisions at $\sqrt{s} = 13$ TeV”, *JHEP* **05** (2021) 290, arXiv:2101.03110 [nucl-ex].
- [74] B. Schenke, C. Shen, and P. Tribedy, “Running the gamut of high energy nuclear collisions”, *Phys. Rev. C* **102** (2020) 044905, arXiv:2005.14682 [nucl-th].
- [75] M. Strickland, “Small system studies: A theory overview”, *Nucl. Phys. A* **982** (2019) 92–98, arXiv:1807.07191 [nucl-th].
- [76] C. Loizides, “Experimental overview on small collision systems at the LHC”, *Nucl. Phys. A* **956** (2016) 200–207, arXiv:1602.09138 [nucl-ex].
- [77] J. L. Nagle and W. A. Zajc, “Small System Collectivity in Relativistic Hadronic and Nuclear Collisions”, *Ann. Rev. Nucl. Part. Sci.* **68** (2018) 211–235, arXiv:1801.03477 [nucl-ex].
- [78] A. Bilandzic, R. Snellings, and S. Voloshin, “Flow analysis with cumulants: Direct calculations”, *Phys. Rev. C* **83** (2011) 044913, arXiv:1010.0233 [nucl-ex].
- [79] **ATLAS** Collaboration, M. Aaboud *et al.*, “Correlated long-range mixed-harmonic fluctuations measured in pp, p+Pb and low-multiplicity Pb+Pb collisions with the ATLAS detector”, *Phys. Lett. B* **789** (2019) 444–471, arXiv:1807.02012 [nucl-ex].
- [80] **CMS** Collaboration, S. Chatrchyan *et al.*, “Jet and Underlying Event Properties as a Function of Charged-Particle Multiplicity in Proton–Proton Collisions at $\sqrt{s} = 7$ TeV”, *Eur. Phys. J. C* **73** (2013) 2674, arXiv:1310.4554 [hep-ex].
- [81] **ALICE** Collaboration, B. Abelev *et al.*, “Multiplicity dependence of two-particle azimuthal correlations in pp collisions at the LHC”, *JHEP* **09** (2013) 049, arXiv:1307.1249 [nucl-ex].
- [82] **ALICE** Collaboration, B. Abelev *et al.*, “Multiplicity dependence of jet-like two-particle correlation structures in p–Pb collisions at $\sqrt{s_{\text{NN}}} = 5.02$ TeV”, *Phys. Lett. B* **741** (2015) 38–50, arXiv:1406.5463 [nucl-ex].
- [83] **ALICE** Collaboration, B. Abelev *et al.*, “Long-range angular correlations of π , K and p in p–Pb collisions at $\sqrt{s_{\text{NN}}} = 5.02$ TeV”, *Phys. Lett. B* **726** (2013) 164–177, arXiv:1307.3237 [nucl-ex].
- [84] T. Sjostrand and M. van Zijl, “Multiple Parton-parton Interactions in an Impact Parameter Picture”, *Phys. Lett. B* **188** (1987) 149–154.
- [85] L. Frankfurt, M. Strikman, and C. Weiss, “Dijet production as a centrality trigger for pp collisions at CERN LHC”, *Phys. Rev. D* **69** (2004) 114010, arXiv:hep-ph/0311231.

- [86] L. Frankfurt, M. Strikman, and C. Weiss, “Transverse nucleon structure and diagnostics of hard parton-parton processes at LHC”, *Phys. Rev. D* **83** (2011) 054012, arXiv:1009.2559 [hep-ph].
- [87] CMS Collaboration, S. Chatrchyan *et al.*, “Measurement of the Underlying Event Activity in pp Collisions at $\sqrt{s} = 0.9$ and 7 TeV with the Novel Jet-Area/Median Approach”, *JHEP* **08** (2012) 130, arXiv:1207.2392 [hep-ex].
- [88] CMS Collaboration, S. Chatrchyan *et al.*, “Measurement of the Underlying Event Activity at the LHC with $\sqrt{s} = 7$ TeV and Comparison with $\sqrt{s} = 0.9$ TeV”, *JHEP* **09** (2011) 109, arXiv:1107.0330 [hep-ex].
- [89] ALICE Collaboration, S. Acharya *et al.*, “Underlying-event properties in pp and p–Pb collisions at $\sqrt{s_{NN}} = 5.02$ TeV”, *JHEP* **06** (2023) 023, arXiv:2204.10389 [nucl-ex].
- [90] ALICE Collaboration, K. Aamodt *et al.*, “The ALICE experiment at the CERN LHC”, *JINST* **3** (2008) S08002.
- [91] ALICE Collaboration, B. Abelev *et al.*, “Performance of the ALICE Experiment at the CERN LHC”, *Int. J. Mod. Phys. A* **29** (2014) 1430044, arXiv:1402.4476 [nucl-ex].
- [92] ALICE Collaboration, E. Abbas *et al.*, “Performance of the ALICE VZERO system”, *JINST* **8** (2013) P10016, arXiv:1306.3130 [nucl-ex].
- [93] ALICE Collaboration, K. Aamodt *et al.*, “Alignment of the ALICE Inner Tracking System with cosmic-ray tracks”, *JINST* **5** (2010) P03003, arXiv:1001.0502 [physics.ins-det].
- [94] ALICE Collaboration, B. Abelev *et al.*, “Technical Design Report for the Upgrade of the ALICE Inner Tracking System”, *J. Phys. G* **41** (2014) 087002.
- [95] J. Alme *et al.*, “The ALICE TPC, a large 3-dimensional tracking device with fast readout for ultra-high multiplicity events”, *Nucl. Instrum. Meth. A* **622** (2010) 316–367, arXiv:1001.1950 [physics.ins-det].
- [96] R. Santoro *et al.*, “The ALICE Silicon Pixel Detector: Readiness for the first proton beam”, *JINST* **4** (2009) P03023.
- [97] ALICE Collaboration, J. Adam *et al.*, “ALICE luminosity determination for pp collisions at $\sqrt{s_{NN}} = 13$ TeV”, *ALICE-PUBLIC-2016-002* (Jun, 2016).
<http://cds.cern.ch/record/2160174>.
- [98] ALICE Collaboration, S. Acharya *et al.*, “Pseudorapidity distributions of charged particles as a function of mid- and forward rapidity multiplicities in pp collisions at $\sqrt{s} = 5.02, 7$ and 13 TeV”, *Eur. Phys. J. C* **81** (2021) 630, arXiv:2009.09434 [nucl-ex].
- [99] M. Ivanov, I. Belikov, P. Hristov, and K. Safarik, “Track reconstruction in high density environment”, *Nucl. Instrum. Meth. A* **566** (2006) 70–74.
- [100] ALICE Collaboration, “The ALICE definition of primary particles”, *ALICE-PUBLIC-2017-005* (2017). <https://cds.cern.ch/record/2270008>.
- [101] ALICE Collaboration, S. Acharya *et al.*, “Transverse momentum spectra and nuclear modification factors of charged particles in pp, p–Pb and Pb–Pb collisions at the LHC”, *JHEP* **11** (2018) 013, arXiv:1802.09145 [nucl-ex].

- [102] R. Brun, F. Bruyant, F. Carminati, S. Giani, M. Maire, A. McPherson, G. Patrick, and L. Urban, “GEANT: Detector Description and Simulation Tool; Oct 1994”, *CERN-W5013* (1993) .
<http://cds.cern.ch/record/1082634>. Long Writeup W5013.
- [103] **ALICE** Collaboration, S. Acharya *et al.*, “Transverse momentum spectra and nuclear modification factors of charged particles in Xe–Xe collisions at $\sqrt{s_{\text{NN}}} = 5.44 \text{ TeV}$ ”, *Phys. Lett. B* **788** (2019) 166–179, arXiv:1805.04399 [nucl-ex].
- [104] G. I. Kopylov, “Like particle correlations as a tool to study the multiple production mechanism”, *Phys. Lett. B* **50** (1974) 472–474.
- [105] **ALICE** Collaboration, J. Adam *et al.*, “Anomalous evolution of the near-side jet peak shape in Pb–Pb collisions at $\sqrt{s_{\text{NN}}} = 2.76 \text{ TeV}$ ”, *Phys. Rev. Lett.* **119** (2017) 102301, arXiv:1609.06643 [nucl-ex].
- [106] **PHENIX** Collaboration, S. S. Adler *et al.*, “Jet properties from dihadron correlations in p+p collisions at $\sqrt{s} = 200 \text{ GeV}$ ”, *Phys. Rev. D* **74** (2006) 072002, arXiv:hep-ex/0605039.
- [107] N. N. Ajitanand, J. M. Alexander, P. Chung, W. G. Holzmann, M. Issah, R. A. Lacey, A. Shevel, A. Taranenko, and P. Danielewicz, “Decomposition of harmonic and jet contributions to particle-pair correlations at ultra-relativistic energies”, *Phys. Rev.* **C72** (2005) 011902, arXiv:nucl-ex/0501025 [nucl-ex].
- [108] **PHENIX** Collaboration, A. Adare *et al.*, “Pseudorapidity Dependence of Particle Production and Elliptic Flow in Asymmetric Nuclear Collisions of p+Al, p+Au, d+Au, and ${}^3\text{He}+\text{Au}$ at $\sqrt{s_{\text{NN}}} = 200 \text{ GeV}$ ”, *Phys. Rev. Lett.* **121** (2018) 222301, arXiv:1807.11928 [nucl-ex].
- [109] **ALICE** Collaboration, J. Adam *et al.*, “Pseudorapidity dependence of the anisotropic flow of charged particles in Pb–Pb collisions at $\sqrt{s_{\text{NN}}} = 2.76 \text{ TeV}$ ”, *Phys. Lett. B* **762** (2016) 376–388, arXiv:1605.02035 [nucl-ex].
- [110] P. Skands, S. Carrazza, and J. Rojo, “Tuning PYTHIA 8.1: the Monash 2013 Tune”, *Eur. Phys. J. C* **74** (2014) 3024, arXiv:1404.5630 [hep-ph].
- [111] M. Cacciari, G. P. Salam, and G. Soyez, “The anti- k_t jet clustering algorithm”, *JHEP* **04** (2008) 063, arXiv:0802.1189 [hep-ph].
- [112] M. Cacciari, G. P. Salam, and G. Soyez, “FastJet User Manual”, *Eur. Phys. J. C* **72** (2012) 1896, arXiv:1111.6097 [hep-ph].
- [113] **ALICE** Collaboration, S. Acharya *et al.*, “Charged jet cross section and fragmentation in proton-proton collisions at $\sqrt{s} = 7 \text{ TeV}$ ”, *Phys. Rev. D* **99** (2019) 012016, arXiv:1809.03232 [nucl-ex].
- [114] R. Barlow, “Systematic errors: Facts and fictions”, in *Conference on Advanced Statistical Techniques in Particle Physics*, pp. 134–144. 7, 2002. arXiv:hep-ex/0207026.
- [115] **ALICE** Collaboration, S. Acharya *et al.*, “Production of $\text{K}^*(892)^0$ and $\phi(1020)$ in pp and Pb–Pb collisions at $\sqrt{s_{\text{NN}}} = 5.02 \text{ TeV}$ ”, *Phys. Rev. C* **106** (2022) 034907, arXiv:2106.13113 [nucl-ex].
- [116] **ALICE** Collaboration, S. Acharya *et al.*, “Anisotropic flow of identified particles in Pb–Pb collisions at $\sqrt{s_{\text{NN}}} = 5.02 \text{ TeV}$ ”, *JHEP* **09** (2018) 006, arXiv:1805.04390 [nucl-ex].
- [117] **CDF** Collaboration, T. Affolder *et al.*, “Charged Jet Evolution and the Underlying Event in $p\bar{p}$ Collisions at 1.8 TeV”, *Phys. Rev. D* **65** (2002) 092002.

- [118] ATLAS Collaboration, G. Aad *et al.*, “Measurement of the inclusive jet cross-section in proton-proton collisions at $\sqrt{s} = 7$ TeV using 4.5 fb^{-1} of data with the ATLAS detector”, *JHEP* **02** (2015) 153, arXiv:1410.8857 [hep-ex]. [Erratum: JHEP 09, 141 (2015)].
- [119] CMS Collaboration, V. Khachatryan *et al.*, “Measurement of the inclusive jet cross section in pp collisions at $\sqrt{s} = 2.76$ TeV”, *Eur. Phys. J. C* **76** (2016) 265, arXiv:1512.06212 [hep-ex].
- [120] ATLAS Collaboration, M. Aaboud *et al.*, “Measurement of long-range two-particle azimuthal correlations in Z-boson tagged pp collisions at $\sqrt{s} = 8$ and 13 TeV”, *Eur. Phys. J. C* **80** (2020) 64, arXiv:1906.08290 [nucl-ex].
- [121] J. S. Moreland, J. E. Bernhard, and S. A. Bass, “Alternative ansatz to wounded nucleon and binary collision scaling in high-energy nuclear collisions”, *Phys. Rev. C* **92** (2015) 011901, arXiv:1412.4708 [nucl-th].
- [122] C. Shen, Z. Qiu, H. Song, J. Bernhard, S. Bass, and U. Heinz, “The iEBE-VISHNU code package for relativistic heavy-ion collisions”, *Comput. Phys. Commun.* **199** (2016) 61–85, arXiv:1409.8164 [nucl-th].
- [123] J. B. Rose, J. M. Torres-Rincon, and H. Elfner, “Inclusive and effective bulk viscosities in the hadron gas”, *J. Phys. G* **48** (2020) 015005, arXiv:2005.03647 [hep-ph].
- [124] R. D. Weller and P. Romatschke, “One fluid to rule them all: viscous hydrodynamic description of event-by-event central $p+p$, $p+Pb$ and $Pb+Pb$ collisions at $\sqrt{s} = 5.02$ TeV”, *Phys. Lett. B* **774** (2017) 351–356, arXiv:1701.07145 [nucl-th].
- [125] T. Pierog, I. Karpenko, J. Katzy, E. Yatsenko, and K. Werner, “EPOS LHC: Test of collective hadronization with data measured at the CERN Large Hadron Collider”, *Phys. Rev. C* **92** (2015) 034906, arXiv:1306.0121 [hep-ph].
- [126] S. Ji, M. Virta, T. Kallio, S. H. Lim, and D. J. Kim, “Toward an unbiased flow measurements in LHC pp collisions”, *Phys. Rev. C* **108** (2023) 034909, arXiv:2303.05806 [hep-ph].

A The ALICE Collaboration

- S. Acharya ¹²⁸, D. Adamová ⁸⁷, G. Aglieri Rinella ³³, M. Agnello ³⁰, N. Agrawal ⁵², Z. Ahammed ¹³⁶, S. Ahmad ¹⁶, S.U. Ahn ⁷², I. Ahuja ³⁸, A. Akindinov ¹⁴², M. Al-Turany ⁹⁸, D. Aleksandrov ¹⁴², B. Alessandro ⁵⁷, H.M. Alfanda ⁶, R. Alfaro Molina ⁶⁸, B. Ali ¹⁶, A. Alici ²⁶, N. Alizadehvandchali ¹¹⁷, A. Alkin ³³, J. Alme ²¹, G. Alocco ⁵³, T. Alt ⁶⁵, A.R. Altamura ⁵¹, I. Altsybeev ⁹⁶, J.R. Alvarado ⁴⁵, M.N. Anaam ⁶, C. Andrei ⁴⁶, N. Andreou ¹¹⁶, A. Andronic ¹²⁷, V. Anguelov ⁹⁵, F. Antinori ⁵², P. Antonioli ⁵², N. Apadula ⁷⁵, L. Aphecetche ¹⁰⁴, H. Appelshäuser ⁶⁵, C. Arata ⁷⁴, S. Arcelli ²⁶, M. Aresti ²³, R. Arnaldi ⁵⁷, J.G.M.C.A. Arneiro ¹¹¹, I.C. Arsene ²⁰, M. Arslanbek ¹³⁹, A. Augustinus ³³, R. Averbeck ⁹⁸, M.D. Azmi ¹⁶, H. Baba ¹²⁵, A. Badalà ⁵⁴, J. Bae ¹⁰⁵, Y.W. Baek ⁴¹, X. Bai ¹²¹, R. Bailhache ⁶⁵, Y. Bailung ⁴⁹, A. Balbino ³⁰, A. Baldissari ¹³¹, B. Balis ², D. Banerjee ⁴, Z. Banoo ⁹², R. Barbera ²⁷, F. Barile ³², L. Barioglio ⁹⁶, M. Barlou ⁷⁹, B. Barman ⁴², G.G. Barnaföldi ⁴⁷, L.S. Barnby ⁸⁶, V. Barret ¹²⁸, L. Barreto ¹¹¹, C. Bartels ¹²⁰, K. Barth ³³, E. Bartsch ⁶⁵, N. Bastid ¹²⁸, S. Basu ⁷⁶, G. Batigne ¹⁰⁴, D. Battistini ⁹⁶, B. Batyunya ¹⁴³, D. Bauri ⁴⁸, J.L. Bazo Alba ¹⁰², I.G. Bearden ⁸⁴, C. Beattie ¹³⁹, P. Becht ⁹⁸, D. Behera ⁴⁹, I. Belikov ¹³⁰, A.D.C. Bell Hechavarria ¹²⁷, F. Bellini ²⁶, R. Bellwied ¹¹⁷, S. Belokurova ¹⁴², Y.A.V. Beltran ⁴⁵, G. Bencedi ⁴⁷, S. Beole ²⁵, Y. Berdnikov ¹⁴², A. Berdnikova ⁹⁵, L. Bergmann ⁹⁵, M.G. Besoiu ⁶⁴, L. Betev ³³, P.P. Bhaduri ¹³⁶, A. Bhasin ⁹², M.A. Bhat ⁴, B. Bhattacharjee ⁴², L. Bianchi ²⁵, N. Bianchi ⁵⁰, J. Bielčík ³⁶, J. Bielčíková ⁸⁷, J. Biernat ¹⁰⁸, A.P. Bigot ¹³⁰, A. Bilandzic ⁹⁶, G. Biro ⁴⁷, S. Biswas ⁴, N. Bize ¹⁰⁴, J.T. Blair ¹⁰⁹, D. Blau ¹⁴², M.B. Blidaru ⁹⁸, N. Bluhme ³⁹, C. Blume ⁶⁵, G. Boca ^{22,56}, F. Bock ⁸⁸, T. Bodova ²¹, A. Bogdanov ¹⁴², S. Boi ²³, J. Bok ⁵⁹, L. Boldizsár ⁴⁷, M. Bombara ³⁸, P.M. Bond ³³, G. Bonomi ^{135,56}, H. Borel ¹³¹, A. Borissov ¹⁴², A.G. Borquez Carcamo ⁹⁵, H. Bossi ¹³⁹, E. Botta ²⁵, Y.E.M. Bouziani ⁶⁵, L. Bratrud ⁶⁵, P. Braun-Munzinger ⁹⁸, M. Bregant ¹¹¹, M. Broz ³⁶, G.E. Bruno ^{97,32}, M.D. Buckland ²⁴, D. Budnikov ¹⁴², H. Buesching ⁶⁵, S. Bufalino ³⁰, P. Buhler ¹⁰³, N. Burmasov ¹⁴², Z. Buthelezi ^{69,124}, A. Bylinkin ²¹, S.A. Bysiak ¹⁰⁸, M. Cai ⁶, H. Caines ¹³⁹, A. Caliva ²⁹, E. Calvo Villar ¹⁰², J.M.M. Camacho ¹¹⁰, P. Camerini ²⁴, F.D.M. Canedo ¹¹¹, S.L. Cantway ¹³⁹, M. Carabas ¹¹⁴, A.A. Carballo ³³, F. Carnesecchi ³³, R. Caron ¹²⁹, L.A.D. Carvalho ¹¹¹, J. Castillo Castellanos ¹³¹, F. Catalano ^{33,25}, C. Ceballos Sanchez ¹⁴³, I. Chakaberia ⁷⁵, P. Chakraborty ⁴⁸, S. Chandra ¹³⁶, S. Chapeland ³³, M. Chartier ¹²⁰, S. Chattopadhyay ¹³⁶, S. Chattopadhyay ¹⁰⁰, T. Cheng ^{98,6}, C. Cheshkov ¹²⁹, B. Cheynis ¹²⁹, V. Chibante Barroso ³³, D.D. Chinellato ¹¹², E.S. Chizzali ^{II,96}, J. Cho ⁵⁹, S. Cho ⁵⁹, P. Chochula ³³, D. Choudhury ⁴², P. Christakoglou ⁸⁵, C.H. Christensen ⁸⁴, P. Christiansen ⁷⁶, T. Chujo ¹²⁶, M. Ciacco ³⁰, C. Cicalo ⁵³, F. Cindolo ⁵², M.R. Ciupek ⁹⁸, G. Clai III,52, F. Colamaria ⁵¹, J.S. Colburn ¹⁰¹, D. Colella ^{97,32}, M. Colocci ²⁶, M. Concias ^{IV,33}, G. Conesa Balbastre ⁷⁴, Z. Conesa del Valle ¹³², G. Contin ²⁴, J.G. Contreras ³⁶, M.L. Coquet ¹³¹, P. Cortese ^{134,57}, M.R. Cosentino ¹¹³, F. Costa ³³, S. Costanza ^{22,56}, C. Cot ¹³², J. Crkovská ⁹⁵, P. Crochet ¹²⁸, R. Cruz-Torres ⁷⁵, P. Cui ⁶, A. Dainese ⁵⁵, M.C. Danisch ⁹⁵, A. Danu ⁶⁴, P. Das ⁸¹, P. Das ⁴, S. Das ⁴, A.R. Dash ¹²⁷, S. Dash ⁴⁸, A. De Caro ²⁹, G. de Cataldo ⁵¹, J. de Cuveland ³⁹, A. De Falco ²³, D. De Gruttola ²⁹, N. De Marco ⁵⁷, C. De Martin ²⁴, S. De Pasquale ²⁹, R. Deb ¹³⁵, R. Del Grande ⁹⁶, L. Dello Stritto ²⁹, W. Deng ⁶, P. Dhankher ¹⁹, D. Di Bari ³², A. Di Mauro ³³, B. Diab ¹³¹, R.A. Diaz ^{143,7}, T. Dietel ¹¹⁵, Y. Ding ⁶, J. Ditzel ⁶⁵, R. Divià ³³, D.U. Dixit ¹⁹, Ø. Djupsland ²¹, U. Dmitrieva ¹⁴², A. Dobrin ⁶⁴, B. Dönigus ⁶⁵, J.M. Dubinski ¹³⁷, A. Dubla ⁹⁸, S. Dudi ⁹¹, P. Dupieux ¹²⁸, M. Durkac ¹⁰⁷, N. Dzalaiova ¹³, T.M. Eder ¹²⁷, R.J. Ehlers ⁷⁵, F. Eisenhut ⁶⁵, R. Ejima ⁹³, D. Elia ⁵¹, B. Erazmus ¹⁰⁴, F. Ercolelli ²⁶, B. Espagnon ¹³², G. Eulisse ³³, D. Evans ¹⁰¹, S. Evdokimov ¹⁴², L. Fabbietti ⁹⁶, M. Faggion ²⁸, J. Faivre ⁷⁴, F. Fan ⁶, W. Fan ⁷⁵, A. Fantoni ⁵⁰, M. Fasel ⁸⁸, A. Feliciello ⁵⁷, G. Feofilov ¹⁴², A. Fernández Téllez ⁴⁵, L. Ferrandi ¹¹¹, M.B. Ferrer ³³, A. Ferrero ¹³¹, C. Ferrero ⁵⁷, A. Ferretti ²⁵, V.J.G. Feuillard ⁹⁵, V. Filova ³⁶, D. Finogeev ¹⁴², F.M. Fionda ⁵³, E. Flatland ³³, F. Flor ¹¹⁷, A.N. Flores ¹⁰⁹, S. Foertsch ⁶⁹, I. Fokin ⁹⁵, S. Fokin ¹⁴², E. Fragiocomo ⁵⁸, E. Frajna ⁴⁷, U. Fuchs ³³, N. Funicello ²⁹, C. Furget ⁷⁴, A. Furs ¹⁴², T. Fusayasu ⁹⁹, J.J. Gaardhøje ⁸⁴, M. Gagliardi ²⁵, A.M. Gago ¹⁰², T. Gahlaud ⁴⁸, C.D. Galvan ¹¹⁰, D.R. Gangadharan ¹¹⁷, P. Ganoti ⁷⁹, C. Garabatos ⁹⁸, T. García Chávez ⁴⁵, E. Garcia-Solis ⁹, C. Gargiulo ³³, P. Gasik ⁹⁸, A. Gautam ¹¹⁹, M.B. Gay Ducati ⁶⁷, M. Germain ¹⁰⁴, A. Ghimouz ¹²⁶, C. Ghosh ¹³⁶, M. Giacalone ⁵², G. Gioachin ³⁰, P. Giubellino ^{98,57}, P. Giubilato ²⁸, A.M.C. Glaenzer ¹³¹, P. Glässel ⁹⁵, E. Glimos ¹²³, D.J.Q. Goh ⁷⁷, V. Gonzalez ¹³⁸, P. Gordeev ¹⁴², M. Gorgon ², K. Goswami ⁴⁹, S. Gotovac ³⁴, V. Grabski ⁶⁸, L.K. Graczykowski ¹³⁷, E. Grecka ⁸⁷, A. Grelli ⁶⁰, C. Grigoras ³³, V. Grigoriev ¹⁴², S. Grigoryan ^{143,1}, F. Grossa ³³, J.F. Grosse-Oetringhaus ³³, R. Grossi ⁹⁸, D. Grund ³⁶, N.A. Grunwald ⁹⁵, G.G. Guardiano ¹¹², R. Guernane ⁷⁴, M. Guilbaud ¹⁰⁴,

- K. Gulbrandsen ⁸⁴, T. Gündem ⁶⁵, T. Gunji ¹²⁵, W. Guo ⁶, A. Gupta ⁹², R. Gupta ⁹², R. Gupta ⁴⁹, K. Gwizdziel ¹³⁷, L. Gyulai ⁴⁷, C. Hadjidakis ¹³², F.U. Haider ⁹², S. Haidlova ³⁶, H. Hamagaki ⁷⁷, A. Hamdi ⁷⁵, Y. Han ¹⁴⁰, B.G. Hanley ¹³⁸, R. Hannigan ¹⁰⁹, J. Hansen ⁷⁶, M.R. Haque ¹³⁷, J.W. Harris ¹³⁹, A. Harton ⁹, H. Hassan ¹¹⁸, D. Hatzifotiadou ⁵², P. Hauer ⁴³, L.B. Havener ¹³⁹, S.T. Heckel ⁹⁶, E. Hellbär ⁹⁸, H. Helstrup ³⁵, M. Hemmer ⁶⁵, T. Herman ³⁶, G. Herrera Corral ⁸, F. Herrmann ¹²⁷, S. Herrmann ¹²⁹, K.F. Hetland ³⁵, B. Heybeck ⁶⁵, H. Hillemanns ³³, B. Hippolyte ¹³⁰, F.W. Hoffmann ⁷¹, B. Hofman ⁶⁰, G.H. Hong ¹⁴⁰, M. Horst ⁹⁶, A. Horzyk ², Y. Hou ⁶, P. Hristov ³³, C. Hughes ¹²³, P. Huhn ⁶⁵, L.M. Huhta ¹¹⁸, T.J. Humanic ⁸⁹, A. Hutson ¹¹⁷, D. Hutter ³⁹, R. Ilkaev ¹⁴², H. Ilyas ¹⁴, M. Inaba ¹²⁶, G.M. Innocenti ³³, M. Ippolitov ¹⁴², A. Isakov ^{85,87}, T. Isidori ¹¹⁹, M.S. Islam ¹⁰⁰, M. Ivanov ¹³, M. Ivanov ⁹⁸, V. Ivanov ¹⁴², K.E. Iversen ⁷⁶, M. Jablonski ², B. Jacak ⁷⁵, N. Jacazio ²⁶, P.M. Jacobs ⁷⁵, S. Jadlovska ¹⁰⁷, J. Jadlovsky ¹⁰⁷, S. Jaelani ⁸³, C. Jahnke ¹¹¹, M.J. Jakubowska ¹³⁷, M.A. Janik ¹³⁷, T. Janson ⁷¹, S. Ji ¹⁷, S. Jia ¹⁰, A.A.P. Jimenez ⁶⁶, F. Jonas ^{88,127}, D.M. Jones ¹²⁰, J.M. Jowett ^{33,98}, J. Jung ⁶⁵, M. Jung ⁶⁵, A. Junique ³³, A. Jusko ¹⁰¹, J. Kaewjai ¹⁰⁶, P. Kalinak ⁶¹, A.S. Kalteyer ⁹⁸, A. Kalweit ³³, V. Kaplin ¹⁴², A. Karasu Uysal ⁷³, D. Karatovic ⁹⁰, O. Karavichev ¹⁴², T. Karavicheva ¹⁴², P. Karczmarczyk ¹³⁷, E. Karpechev ¹⁴², M.J. Karwowska ^{33,137}, U. Kebschull ⁷¹, R. Keidel ¹⁴¹, D.L.D. Keijdener ⁶⁰, M. Keil ³³, B. Ketzer ⁴³, S.S. Khade ⁴⁹, A.M. Khan ¹²¹, S. Khan ¹⁶, A. Khanzadeev ¹⁴², Y. Kharlov ¹⁴², A. Khatun ¹¹⁹, A. Khuntia ³⁶, B. Kileng ³⁵, B. Kim ¹⁰⁵, C. Kim ¹⁷, D.J. Kim ¹¹⁸, E.J. Kim ⁷⁰, J. Kim ¹⁴⁰, J.S. Kim ⁴¹, J. Kim ⁵⁹, J. Kim ⁷⁰, M. Kim ¹⁹, S. Kim ¹⁸, T. Kim ¹⁴⁰, K. Kimura ⁹³, S. Kirsch ⁶⁵, I. Kisel ³⁹, S. Kiselev ¹⁴², A. Kisiel ¹³⁷, J.P. Kitowski ², J.L. Klay ⁵, J. Klein ³³, S. Klein ⁷⁵, C. Klein-Bösing ¹²⁷, M. Kleiner ⁶⁵, T. Klemenz ⁹⁶, A. Kluge ³³, A.G. Knospe ¹¹⁷, C. Kobdaj ¹⁰⁶, T. Kollegger ⁹⁸, A. Kondratyev ¹⁴³, N. Kondratyeva ¹⁴², E. Kondratyuk ¹⁴², J. Konig ⁶⁵, S.A. Konigstorfer ⁹⁶, P.J. Konopka ³³, G. Kornakov ¹³⁷, M. Korwieser ⁹⁶, S.D. Koryciak ², A. Kotliarov ⁸⁷, V. Kovalenko ¹⁴², M. Kowalski ¹⁰⁸, V. Kozhuharov ³⁷, I. Králík ⁶¹, A. Kravčáková ³⁸, L. Krcal ^{33,39}, M. Krivda ^{101,61}, F. Krizek ⁸⁷, K. Krizkova Gajdosova ³³, M. Kroesen ⁹⁵, M. Krüger ⁶⁵, D.M. Krupova ³⁶, E. Kryshen ¹⁴², V. Kučera ⁵⁹, C. Kuhn ¹³⁰, P.G. Kuijer ⁸⁵, T. Kumaoka ¹²⁶, D. Kumar ¹³⁶, L. Kumar ⁹¹, N. Kumar ⁹¹, S. Kumar ³², S. Kundu ³³, P. Kurashvili ⁸⁰, A. Kurepin ¹⁴², A.B. Kurepin ¹⁴², A. Kuryakin ¹⁴², S. Kushpil ⁸⁷, V. Kuskov ¹⁴², M.J. Kweon ⁵⁹, Y. Kwon ¹⁴⁰, S.L. La Pointe ³⁹, P. La Rocca ²⁷, A. Lakerathok ¹⁰⁶, M. Lamanna ³³, A.R. Landou ^{74,116}, R. Langoy ¹²², P. Larionov ³³, E. Laudi ³³, L. Lautner ^{33,96}, R. Lavicka ¹⁰³, R. Lea ^{135,56}, H. Lee ¹⁰⁵, I. Legrand ⁴⁶, G. Legras ¹²⁷, J. Lehrbach ³⁹, T.M. Lelek ², R.C. Lemmon ⁸⁶, I. León Monzón ¹¹⁰, M.M. Lesch ⁹⁶, E.D. Lesser ¹⁹, P. Lévai ⁴⁷, X. Li ¹⁰, J. Lien ¹²², R. Lietava ¹⁰¹, I. Likmeta ¹¹⁷, B. Lim ²⁵, S.H. Lim ¹⁷, V. Lindenstruth ³⁹, A. Lindner ⁴⁶, C. Lippmann ⁹⁸, D.H. Liu ⁶, J. Liu ¹²⁰, G.S.S. Liveraro ¹¹², I.M. Lofnes ²¹, C. Loizides ⁸⁸, S. Lokos ¹⁰⁸, J. Lömkér ⁶⁰, P. Loncar ³⁴, X. Lopez ¹²⁸, E. López Torres ⁷, P. Lu ^{98,121}, F.V. Lugo ⁶⁸, J.R. Luhder ¹²⁷, M. Lunardon ²⁸, G. Luparello ⁵⁸, Y.G. Ma ⁴⁰, M. Mager ³³, A. Maire ¹³⁰, E.M. Majerz ², M.V. Makariev ³⁷, M. Malaev ¹⁴², G. Malfattore ²⁶, N.M. Malik ⁹², Q.W. Malik ²⁰, S.K. Malik ⁹², L. Malinina ^{I,VII,143}, D. Mallick ^{132,81}, N. Mallick ⁴⁹, G. Mandaglio ^{31,54}, S.K. Mandal ⁸⁰, V. Manko ¹⁴², F. Manso ¹²⁸, V. Manzari ⁵¹, Y. Mao ⁶, R.W. Marcjan ², G.V. Margagliotti ²⁴, A. Margotti ⁵², A. Marín ⁹⁸, C. Markert ¹⁰⁹, P. Martinengo ³³, M.I. Martínez ⁴⁵, G. Martínez García ¹⁰⁴, M.P.P. Martins ¹¹¹, S. Masciocchi ⁹⁸, M. Masera ²⁵, A. Masoni ⁵³, L. Massacrier ¹³², O. Massen ⁶⁰, A. Mastroserio ^{133,51}, O. Matonoha ⁷⁶, S. Mattiazzo ²⁸, A. Matyja ¹⁰⁸, C. Mayer ¹⁰⁸, A.L. Mazuecos ³³, F. Mazzaschi ²⁵, M. Mazzilli ³³, J.E. Mdhluli ¹²⁴, Y. Melikyan ⁴⁴, A. Menchaca-Rocha ⁶⁸, J.E.M. Mendez ⁶⁶, E. Meninno ¹⁰³, A.S. Menon ¹¹⁷, M. Meres ¹³, S. Mhlanga ^{115,69}, Y. Miake ¹²⁶, L. Micheletti ³³, D.L. Mihaylov ⁹⁶, K. Mikhaylov ^{143,142}, A.N. Mishra ⁴⁷, D. Miśkowiec ⁹⁸, A. Modak ⁴, B. Mohanty ⁸¹, M. Mohisin Khan ^{V,16}, M.A. Molander ⁴⁴, S. Monira ¹³⁷, C. Mordasini ¹¹⁸, D.A. Moreira De Godoy ¹²⁷, I. Morozov ¹⁴², A. Morsch ³³, T. Mrnjavac ³³, V. Muccifora ⁵⁰, S. Muhuri ¹³⁶, J.D. Mulligan ⁷⁵, A. Mulliri ²³, M.G. Munhoz ¹¹¹, R.H. Munzer ⁶⁵, H. Murakami ¹²⁵, S. Murray ¹¹⁵, L. Musa ³³, J. Musinsky ⁶¹, J.W. Myrcha ¹³⁷, B. Naik ¹²⁴, A.I. Nambrath ¹⁹, B.K. Nandi ⁴⁸, R. Nania ⁵², E. Nappi ⁵¹, A.F. Nassirpour ¹⁸, A. Nath ⁹⁵, C. Nattrass ¹²³, M.N. Naydenov ³⁷, A. Neagu ²⁰, A. Negru ¹¹⁴, E. Nekrasova ¹⁴², L. Nellen ⁶⁶, R. Nepeivoda ⁷⁶, S. Nese ²⁰, G. Neskovic ³⁹, N. Nicassio ⁵¹, B.S. Nielsen ⁸⁴, E.G. Nielsen ⁸⁴, S. Nikolaev ¹⁴², S. Nikulin ¹⁴², V. Nikulin ¹⁴², F. Noferini ⁵², S. Noh ¹², P. Nomokonov ¹⁴³, J. Norman ¹²⁰, N. Novitzky ⁸⁸, P. Nowakowski ¹³⁷, A. Nyanin ¹⁴², J. Nystrand ²¹, M. Ogino ⁷⁷, S. Oh ¹⁸, A. Ohlson ⁷⁶, V.A. Okorokov ¹⁴², J. Oleniacz ¹³⁷, A.C. Oliveira Da Silva ¹²³, A. Onnerstad ¹¹⁸, C. Oppedisano ⁵⁷, A. Ortiz Velasquez ⁶⁶, J. Otwinowski ¹⁰⁸, M. Oya ⁹³, K. Oyama ⁷⁷, Y. Pachmayer ⁹⁵, S. Padhan ⁴⁸, D. Pagano ^{135,56}, G. Paić ⁶⁶, S. Paisano-Guzmán ⁴⁵,

- A. Palasciano ⁵¹, S. Panebianco ¹³¹, H. Park ¹²⁶, H. Park ¹⁰⁵, J. Park ⁵⁹, J.E. Parkkila ³³, Y. Patley ⁴⁸, R.N. Patra ⁹², B. Paul ²³, H. Pei ⁶, T. Peitzmann ⁶⁰, X. Peng ¹¹, M. Pennisi ²⁵, S. Perciballi ²⁵, D. Peresunko ¹⁴², G.M. Perez ⁷, Y. Pestov ¹⁴², V. Petrov ¹⁴², M. Petrovici ⁴⁶, R.P. Pezzi ^{104,67}, S. Piano ⁵⁸, M. Pikna ¹³, P. Pillot ¹⁰⁴, O. Pinazza ^{52,33}, L. Pinsky ¹¹⁷, C. Pinto ⁹⁶, S. Pisano ⁵⁰, M. Płoskoń ⁷⁵, M. Planinic ⁹⁰, F. Pliquet ⁶⁵, M.G. Poghosyan ⁸⁸, B. Polichtchouk ¹⁴², S. Politano ³⁰, N. Poljak ⁹⁰, A. Pop ⁴⁶, S. Porteboeuf-Houssais ¹²⁸, V. Pozdniakov ¹⁴³, I.Y. Pozos ⁴⁵, K.K. Pradhan ⁴⁹, S.K. Prasad ⁴, S. Prasad ⁴⁹, R. Preghenella ⁵², F. Prino ⁵⁷, C.A. Pruneau ¹³⁸, I. Pshenichnov ¹⁴², M. Puccio ³³, S. Pucillo ²⁵, Z. Pugelova ¹⁰⁷, S. Qiu ⁸⁵, L. Quaglia ²⁵, S. Ragoni ¹⁵, A. Rai ¹³⁹, A. Rakotozafindrabe ¹³¹, L. Ramello ^{134,57}, F. Rami ¹³⁰, T.A. Rancien ⁷⁴, M. Rasa ²⁷, S.S. Räsänen ⁴⁴, R. Rath ⁵², M.P. Rauch ²¹, I. Ravasenga ⁸⁵, K.F. Read ^{88,123}, C. Reckziegel ¹¹³, A.R. Redelbach ³⁹, K. Redlich ^{VI,80}, C.A. Reetz ⁹⁸, H.D. Regules-Medel ⁴⁵, A. Rehman ²¹, F. Reidt ³³, H.A. Reme-Ness ³⁵, Z. Rescakova ³⁸, K. Reygers ⁹⁵, A. Riabov ¹⁴², V. Riabov ¹⁴², R. Ricci ²⁹, M. Richter ²⁰, A.A. Riedel ⁹⁶, W. Riegler ³³, A.G. Riffero ²⁵, C. Ristea ⁶⁴, M.V. Rodriguez ³³, M. Rodríguez Cahuantzi ⁴⁵, S.A. Rodríguez Ramírez ⁴⁵, K. Røed ²⁰, R. Rogalev ¹⁴², E. Rogochaya ¹⁴³, T.S. Rogoschinski ⁶⁵, D. Rohr ³³, D. Röhrich ²¹, P.F. Rojas ⁴⁵, S. Rojas Torres ³⁶, P.S. Rokita ¹³⁷, G. Romanenko ²⁶, F. Ronchetti ⁵⁰, A. Rosano ^{31,54}, E.D. Rosas ⁶⁶, K. Roslon ¹³⁷, A. Rossi ⁵⁵, A. Roy ⁴⁹, S. Roy ⁴⁸, N. Rubini ²⁶, D. Ruggiano ¹³⁷, R. Rui ²⁴, P.G. Russek ², R. Russo ⁸⁵, A. Rustamov ⁸², E. Ryabinkin ¹⁴², Y. Ryabov ¹⁴², A. Rybicki ¹⁰⁸, H. Rytkonen ¹¹⁸, J. Ryu ¹⁷, W. Rzesz ¹³⁷, O.A.M. Saarimaki ⁴⁴, S. Sadhu ³², S. Sadovsky ¹⁴², J. Saetre ²¹, K. Šafářík ³⁶, P. Saha ⁴², S.K. Saha ⁴, S. Saha ⁸¹, B. Sahoo ⁴⁸, B. Sahoo ⁴⁹, R. Sahoo ⁴⁹, S. Sahoo ⁶², D. Sahu ⁴⁹, P.K. Sahu ⁶², J. Saini ¹³⁶, K. Sajdakova ³⁸, S. Sakai ¹²⁶, M.P. Salvan ⁹⁸, S. Sambyal ⁹², D. Samitz ¹⁰³, I. Sanna ^{33,96}, T.B. Saramela ¹¹¹, P. Sarma ⁴², V. Sarritzu ²³, V.M. Sarti ⁹⁶, M.H.P. Sas ³³, S. Sawan ⁸¹, J. Schambach ⁸⁸, H.S. Scheid ⁶⁵, C. Schiaua ⁴⁶, R. Schicker ⁹⁵, F. Schlepper ⁹⁵, A. Schmah ⁹⁸, C. Schmidt ⁹⁸, H.R. Schmidt ⁹⁴, M.O. Schmidt ³³, M. Schmidt ⁹⁴, N.V. Schmidt ⁸⁸, A.R. Schmier ¹²³, R. Schotter ¹³⁰, A. Schröter ³⁹, J. Schukraft ³³, K. Schweda ⁹⁸, G. Scioli ²⁶, E. Scomparin ⁵⁷, J.E. Seger ¹⁵, Y. Sekiguchi ¹²⁵, D. Sekihata ¹²⁵, M. Selina ⁸⁵, I. Selyuzhenkov ⁹⁸, S. Senyukov ¹³⁰, J.J. Seo ^{95,59}, D. Serebryakov ¹⁴², L. Šerkšnytė ⁹⁶, A. Sevcenco ⁶⁴, T.J. Shaba ⁶⁹, A. Shabetai ¹⁰⁴, R. Shahoyan ³³, A. Shangaraev ¹⁴², A. Sharma ⁹¹, B. Sharma ⁹², D. Sharma ⁴⁸, H. Sharma ⁵⁵, M. Sharma ⁹², S. Sharma ⁷⁷, S. Sharma ⁹², U. Sharma ⁹², A. Shatat ¹³², O. Sheibani ¹¹⁷, K. Shigaki ⁹³, M. Shimomura ⁷⁸, J. Shin ¹², S. Shirinkin ¹⁴², Q. Shou ⁴⁰, Y. Sibiriak ¹⁴², S. Siddhanta ⁵³, T. Siemianczuk ⁸⁰, T.F. Silva ¹¹¹, D. Silvermyr ⁷⁶, T. Simantathammakul ¹⁰⁶, R. Simeonov ³⁷, B. Singh ⁹², B. Singh ⁹⁶, K. Singh ⁴⁹, R. Singh ⁸¹, R. Singh ⁹², R. Singh ⁴⁹, S. Singh ¹⁶, V.K. Singh ¹³⁶, V. Singhal ¹³⁶, T. Sinha ¹⁰⁰, B. Sitar ¹³, M. Sitta ^{134,57}, T.B. Skaali ²⁰, G. Skorodumovs ⁹⁵, M. Slupecki ⁴⁴, N. Smirnov ¹³⁹, R.J.M. Snellings ⁶⁰, E.H. Solheim ²⁰, J. Song ¹⁷, C. Sonnabend ^{33,98}, F. Soramel ²⁸, A.B. Soto-hernandez ⁸⁹, R. Spijkers ⁸⁵, I. Sputowska ¹⁰⁸, J. Staa ⁷⁶, J. Stachel ⁹⁵, I. Stan ⁶⁴, P.J. Steffanic ¹²³, S.F. Stiefelmaier ⁹⁵, D. Stocco ¹⁰⁴, I. Storehaug ²⁰, P. Stratmann ¹²⁷, S. Strazzi ²⁶, A. Sturniolo ^{31,54}, C.P. Stylianidis ⁸⁵, A.A.P. Suwaide ¹¹¹, C. Suire ¹³², M. Sukhanov ¹⁴², M. Suljic ³³, R. Sultanov ¹⁴², V. Sumberia ⁹², S. Sumowidago ⁸³, S. Swain ⁶², I. Szarka ¹³, M. Szymkowski ¹³⁷, S.F. Taghavi ⁹⁶, G. Taillepied ⁹⁸, J. Takahashi ¹¹², G.J. Tambave ⁸¹, S. Tang ⁶, Z. Tang ¹²¹, J.D. Tapia Takaki ¹¹⁹, N. Tapus ¹¹⁴, L.A. Tarasovicova ¹²⁷, M.G. Tarzila ⁴⁶, G.F. Tassielli ³², A. Tauro ³³, A. Tavira García ¹³², G. Tejeda Muñoz ⁴⁵, A. Telesca ³³, L. Terlizzi ²⁵, C. Terrevoli ¹¹⁷, S. Thakur ⁴, D. Thomas ¹⁰⁹, A. Tikhonov ¹⁴², N. Tiltmann ¹²⁷, A.R. Timmins ¹¹⁷, M. Tkacik ¹⁰⁷, T. Tkacik ¹⁰⁷, A. Toia ⁶⁵, R. Tokumoto ⁹³, K. Tomohiro ⁹³, N. Topilskaya ¹⁴², M. Toppi ⁵⁰, T. Tork ¹³², V.V. Torres ¹⁰⁴, A.G. Torres Ramos ³², A. Trifiró ^{31,54}, A.S. Triolo ^{33,31,54}, S. Tripathy ⁵², T. Tripathy ⁴⁸, S. Trogolo ³³, V. Trubnikov ³, W.H. Trzaska ¹¹⁸, T.P. Trzciński ¹³⁷, A. Tumkin ¹⁴², R. Turrisi ⁵⁵, T.S. Tveter ²⁰, K. Ullaland ²¹, B. Ulukutlu ⁹⁶, A. Uras ¹²⁹, G.L. Usai ²³, M. Vala ³⁸, N. Valle ²², L.V.R. van Doremalen ⁶⁰, M. van Leeuwen ⁸⁵, C.A. van Veen ⁹⁵, R.J.G. van Weelden ⁸⁵, P. Vande Vyvre ³³, D. Varga ⁴⁷, Z. Varga ⁴⁷, P. Vargas Torres ⁶⁶, M. Vasileiou ⁷⁹, A. Vasiliev ¹⁴², O. Vázquez Doce ⁵⁰, O. Vazquez Rueda ¹¹⁷, V. Vechernin ¹⁴², E. Vercellin ²⁵, S. Vergara Limón ⁴⁵, R. Verma ⁴⁸, L. Vermunt ⁹⁸, R. Vértesi ⁴⁷, M. Verweij ⁶⁰, L. Vickovic ³⁴, Z. Vilakazi ¹²⁴, O. Villalobos Baillie ¹⁰¹, A. Villani ²⁴, A. Vinogradov ¹⁴², T. Virgili ²⁹, M.M.O. Virta ¹¹⁸, V. Vislavicius ⁷⁶, A. Vodopyanov ¹⁴³, B. Volkel ³³, M.A. Völkl ⁹⁵, K. Voloshin ¹⁴², S.A. Voloshin ¹³⁸, G. Volpe ³², B. von Haller ³³, I. Vorobyev ⁹⁶, N. Vozniuk ¹⁴², J. Vrláková ³⁸, J. Wan ⁴⁰, C. Wang ⁴⁰, D. Wang ⁴⁰, Y. Wang ⁴⁰, Y. Wang ⁶, A. Wegrynek ³³, F.T. Weiglhofer ³⁹, S.C. Wenzel ³³, J.P. Wessels ¹²⁷, J. Wiechula ⁶⁵, J. Wikne ²⁰, G. Wilk ⁸⁰, J. Wilkinson ⁹⁸, G.A. Willems ¹²⁷, B. Windelband ⁹⁵, M. Winn ¹³¹, J.R. Wright ¹⁰⁹, W. Wu ⁴⁰, Y. Wu ¹²¹, R. Xu ⁶, A. Yadav ⁴³, A.K. Yadav ¹³⁶,

S. Yalcin ⁷³, Y. Yamaguchi ⁹³, S. Yang²¹, S. Yano ⁹³, Z. Yin ⁶, I.-K. Yoo ¹⁷, J.H. Yoon ⁵⁹, H. Yu¹²,
 S. Yuan²¹, A. Yuncu ⁹⁵, V. Zaccolo ²⁴, C. Zampolli ³³, F. Zanone ⁹⁵, N. Zardoshti ³³,
 A. Zarochentsev ¹⁴², P. Závada ⁶³, N. Zaviyalov¹⁴², M. Zhalov ¹⁴², B. Zhang ⁶, C. Zhang ¹³¹,
 L. Zhang ⁴⁰, S. Zhang ⁴⁰, X. Zhang ⁶, Y. Zhang¹²¹, Z. Zhang ⁶, M. Zhao ¹⁰, V. Zherebchevskii ¹⁴²,
 Y. Zhi¹⁰, D. Zhou ⁶, Y. Zhou ⁸⁴, J. Zhu ^{55,6}, Y. Zhu⁶, S.C. Zugravel ⁵⁷, N. Zurlo ^{135,56}

Affiliation Notes

^I Deceased

^{II} Also at: Max-Planck-Institut fur Physik, Munich, Germany

^{III} Also at: Italian National Agency for New Technologies, Energy and Sustainable Economic Development (ENEA), Bologna, Italy

^{IV} Also at: Dipartimento DET del Politecnico di Torino, Turin, Italy

^V Also at: Department of Applied Physics, Aligarh Muslim University, Aligarh, India

^{VI} Also at: Institute of Theoretical Physics, University of Wroclaw, Poland

^{VII} Also at: An institution covered by a cooperation agreement with CERN

Collaboration Institutes

¹ A.I. Alikhanyan National Science Laboratory (Yerevan Physics Institute) Foundation, Yerevan, Armenia

² AGH University of Krakow, Cracow, Poland

³ Bogolyubov Institute for Theoretical Physics, National Academy of Sciences of Ukraine, Kiev, Ukraine

⁴ Bose Institute, Department of Physics and Centre for Astroparticle Physics and Space Science (CAPSS), Kolkata, India

⁵ California Polytechnic State University, San Luis Obispo, California, United States

⁶ Central China Normal University, Wuhan, China

⁷ Centro de Aplicaciones Tecnológicas y Desarrollo Nuclear (CEADEN), Havana, Cuba

⁸ Centro de Investigación y de Estudios Avanzados (CINVESTAV), Mexico City and Mérida, Mexico

⁹ Chicago State University, Chicago, Illinois, United States

¹⁰ China Institute of Atomic Energy, Beijing, China

¹¹ China University of Geosciences, Wuhan, China

¹² Chungbuk National University, Cheongju, Republic of Korea

¹³ Comenius University Bratislava, Faculty of Mathematics, Physics and Informatics, Bratislava, Slovak Republic

¹⁴ COMSATS University Islamabad, Islamabad, Pakistan

¹⁵ Creighton University, Omaha, Nebraska, United States

¹⁶ Department of Physics, Aligarh Muslim University, Aligarh, India

¹⁷ Department of Physics, Pusan National University, Pusan, Republic of Korea

¹⁸ Department of Physics, Sejong University, Seoul, Republic of Korea

¹⁹ Department of Physics, University of California, Berkeley, California, United States

²⁰ Department of Physics, University of Oslo, Oslo, Norway

²¹ Department of Physics and Technology, University of Bergen, Bergen, Norway

²² Dipartimento di Fisica, Università di Pavia, Pavia, Italy

²³ Dipartimento di Fisica dell’Università and Sezione INFN, Cagliari, Italy

²⁴ Dipartimento di Fisica dell’Università and Sezione INFN, Trieste, Italy

²⁵ Dipartimento di Fisica dell’Università and Sezione INFN, Turin, Italy

²⁶ Dipartimento di Fisica e Astronomia dell’Università and Sezione INFN, Bologna, Italy

²⁷ Dipartimento di Fisica e Astronomia dell’Università and Sezione INFN, Catania, Italy

²⁸ Dipartimento di Fisica e Astronomia dell’Università and Sezione INFN, Padova, Italy

²⁹ Dipartimento di Fisica ‘E.R. Caianiello’ dell’Università and Gruppo Collegato INFN, Salerno, Italy

³⁰ Dipartimento DISAT del Politecnico and Sezione INFN, Turin, Italy

³¹ Dipartimento di Scienze MIFT, Università di Messina, Messina, Italy

³² Dipartimento Interateneo di Fisica ‘M. Merlin’ and Sezione INFN, Bari, Italy

³³ European Organization for Nuclear Research (CERN), Geneva, Switzerland

³⁴ Faculty of Electrical Engineering, Mechanical Engineering and Naval Architecture, University of Split, Split, Croatia

³⁵ Faculty of Engineering and Science, Western Norway University of Applied Sciences, Bergen, Norway

- ³⁶ Faculty of Nuclear Sciences and Physical Engineering, Czech Technical University in Prague, Prague, Czech Republic
³⁷ Faculty of Physics, Sofia University, Sofia, Bulgaria
³⁸ Faculty of Science, P.J. Šafárik University, Košice, Slovak Republic
³⁹ Frankfurt Institute for Advanced Studies, Johann Wolfgang Goethe-Universität Frankfurt, Frankfurt, Germany
⁴⁰ Fudan University, Shanghai, China
⁴¹ Gangneung-Wonju National University, Gangneung, Republic of Korea
⁴² Gauhati University, Department of Physics, Guwahati, India
⁴³ Helmholtz-Institut für Strahlen- und Kernphysik, Rheinische Friedrich-Wilhelms-Universität Bonn, Bonn, Germany
⁴⁴ Helsinki Institute of Physics (HIP), Helsinki, Finland
⁴⁵ High Energy Physics Group, Universidad Autónoma de Puebla, Puebla, Mexico
⁴⁶ Horia Hulubei National Institute of Physics and Nuclear Engineering, Bucharest, Romania
⁴⁷ HUN-REN Wigner Research Centre for Physics, Budapest, Hungary
⁴⁸ Indian Institute of Technology Bombay (IIT), Mumbai, India
⁴⁹ Indian Institute of Technology Indore, Indore, India
⁵⁰ INFN, Laboratori Nazionali di Frascati, Frascati, Italy
⁵¹ INFN, Sezione di Bari, Bari, Italy
⁵² INFN, Sezione di Bologna, Bologna, Italy
⁵³ INFN, Sezione di Cagliari, Cagliari, Italy
⁵⁴ INFN, Sezione di Catania, Catania, Italy
⁵⁵ INFN, Sezione di Padova, Padova, Italy
⁵⁶ INFN, Sezione di Pavia, Pavia, Italy
⁵⁷ INFN, Sezione di Torino, Turin, Italy
⁵⁸ INFN, Sezione di Trieste, Trieste, Italy
⁵⁹ Inha University, Incheon, Republic of Korea
⁶⁰ Institute for Gravitational and Subatomic Physics (GRASP), Utrecht University/Nikhef, Utrecht, Netherlands
⁶¹ Institute of Experimental Physics, Slovak Academy of Sciences, Košice, Slovak Republic
⁶² Institute of Physics, Homi Bhabha National Institute, Bhubaneswar, India
⁶³ Institute of Physics of the Czech Academy of Sciences, Prague, Czech Republic
⁶⁴ Institute of Space Science (ISS), Bucharest, Romania
⁶⁵ Institut für Kernphysik, Johann Wolfgang Goethe-Universität Frankfurt, Frankfurt, Germany
⁶⁶ Instituto de Ciencias Nucleares, Universidad Nacional Autónoma de México, Mexico City, Mexico
⁶⁷ Instituto de Física, Universidade Federal do Rio Grande do Sul (UFRGS), Porto Alegre, Brazil
⁶⁸ Instituto de Física, Universidad Nacional Autónoma de México, Mexico City, Mexico
⁶⁹ iThemba LABS, National Research Foundation, Somerset West, South Africa
⁷⁰ Jeonbuk National University, Jeonju, Republic of Korea
⁷¹ Johann-Wolfgang-Goethe Universität Frankfurt Institut für Informatik, Fachbereich Informatik und Mathematik, Frankfurt, Germany
⁷² Korea Institute of Science and Technology Information, Daejeon, Republic of Korea
⁷³ KTO Karatay University, Konya, Turkey
⁷⁴ Laboratoire de Physique Subatomique et de Cosmologie, Université Grenoble-Alpes, CNRS-IN2P3, Grenoble, France
⁷⁵ Lawrence Berkeley National Laboratory, Berkeley, California, United States
⁷⁶ Lund University Department of Physics, Division of Particle Physics, Lund, Sweden
⁷⁷ Nagasaki Institute of Applied Science, Nagasaki, Japan
⁷⁸ Nara Women's University (NWU), Nara, Japan
⁷⁹ National and Kapodistrian University of Athens, School of Science, Department of Physics , Athens, Greece
⁸⁰ National Centre for Nuclear Research, Warsaw, Poland
⁸¹ National Institute of Science Education and Research, Homi Bhabha National Institute, Jatni, India
⁸² National Nuclear Research Center, Baku, Azerbaijan
⁸³ National Research and Innovation Agency - BRIN, Jakarta, Indonesia
⁸⁴ Niels Bohr Institute, University of Copenhagen, Copenhagen, Denmark
⁸⁵ Nikhef, National institute for subatomic physics, Amsterdam, Netherlands
⁸⁶ Nuclear Physics Group, STFC Daresbury Laboratory, Daresbury, United Kingdom
⁸⁷ Nuclear Physics Institute of the Czech Academy of Sciences, Husinec-Řež, Czech Republic

- ⁸⁸ Oak Ridge National Laboratory, Oak Ridge, Tennessee, United States
⁸⁹ Ohio State University, Columbus, Ohio, United States
⁹⁰ Physics department, Faculty of science, University of Zagreb, Zagreb, Croatia
⁹¹ Physics Department, Panjab University, Chandigarh, India
⁹² Physics Department, University of Jammu, Jammu, India
⁹³ Physics Program and International Institute for Sustainability with Knotted Chiral Meta Matter (SKCM2), Hiroshima University, Hiroshima, Japan
⁹⁴ Physikalischs Institut, Eberhard-Karls-Universität Tübingen, Tübingen, Germany
⁹⁵ Physikalischs Institut, Ruprecht-Karls-Universität Heidelberg, Heidelberg, Germany
⁹⁶ Physik Department, Technische Universität München, Munich, Germany
⁹⁷ Politecnico di Bari and Sezione INFN, Bari, Italy
⁹⁸ Research Division and ExtreMe Matter Institute EMMI, GSI Helmholtzzentrum für Schwerionenforschung GmbH, Darmstadt, Germany
⁹⁹ Saga University, Saga, Japan
¹⁰⁰ Saha Institute of Nuclear Physics, Homi Bhabha National Institute, Kolkata, India
¹⁰¹ School of Physics and Astronomy, University of Birmingham, Birmingham, United Kingdom
¹⁰² Sección Física, Departamento de Ciencias, Pontificia Universidad Católica del Perú, Lima, Peru
¹⁰³ Stefan Meyer Institut für Subatomare Physik (SMI), Vienna, Austria
¹⁰⁴ SUBATECH, IMT Atlantique, Nantes Université, CNRS-IN2P3, Nantes, France
¹⁰⁵ Sungkyunkwan University, Suwon City, Republic of Korea
¹⁰⁶ Suranaree University of Technology, Nakhon Ratchasima, Thailand
¹⁰⁷ Technical University of Košice, Košice, Slovak Republic
¹⁰⁸ The Henryk Niewodniczanski Institute of Nuclear Physics, Polish Academy of Sciences, Cracow, Poland
¹⁰⁹ The University of Texas at Austin, Austin, Texas, United States
¹¹⁰ Universidad Autónoma de Sinaloa, Culiacán, Mexico
¹¹¹ Universidade de São Paulo (USP), São Paulo, Brazil
¹¹² Universidade Estadual de Campinas (UNICAMP), Campinas, Brazil
¹¹³ Universidade Federal do ABC, Santo Andre, Brazil
¹¹⁴ Universitatea Nationala de Stiinta si Tehnologie Politehnica Bucuresti, Bucharest, Romania
¹¹⁵ University of Cape Town, Cape Town, South Africa
¹¹⁶ University of Derby, Derby, United Kingdom
¹¹⁷ University of Houston, Houston, Texas, United States
¹¹⁸ University of Jyväskylä, Jyväskylä, Finland
¹¹⁹ University of Kansas, Lawrence, Kansas, United States
¹²⁰ University of Liverpool, Liverpool, United Kingdom
¹²¹ University of Science and Technology of China, Hefei, China
¹²² University of South-Eastern Norway, Kongsberg, Norway
¹²³ University of Tennessee, Knoxville, Tennessee, United States
¹²⁴ University of the Witwatersrand, Johannesburg, South Africa
¹²⁵ University of Tokyo, Tokyo, Japan
¹²⁶ University of Tsukuba, Tsukuba, Japan
¹²⁷ Universität Münster, Institut für Kernphysik, Münster, Germany
¹²⁸ Université Clermont Auvergne, CNRS/IN2P3, LPC, Clermont-Ferrand, France
¹²⁹ Université de Lyon, CNRS/IN2P3, Institut de Physique des 2 Infinis de Lyon, Lyon, France
¹³⁰ Université de Strasbourg, CNRS, IPHC UMR 7178, F-67000 Strasbourg, France, Strasbourg, France
¹³¹ Université Paris-Saclay, Centre d'Etudes de Saclay (CEA), IRFU, Département de Physique Nucléaire (DPhN), Saclay, France
¹³² Université Paris-Saclay, CNRS/IN2P3, IJCLab, Orsay, France
¹³³ Università degli Studi di Foggia, Foggia, Italy
¹³⁴ Università del Piemonte Orientale, Vercelli, Italy
¹³⁵ Università di Brescia, Brescia, Italy
¹³⁶ Variable Energy Cyclotron Centre, Homi Bhabha National Institute, Kolkata, India
¹³⁷ Warsaw University of Technology, Warsaw, Poland
¹³⁸ Wayne State University, Detroit, Michigan, United States
¹³⁹ Yale University, New Haven, Connecticut, United States
¹⁴⁰ Yonsei University, Seoul, Republic of Korea

¹⁴¹ Zentrum für Technologie und Transfer (ZTT), Worms, Germany

¹⁴² Affiliated with an institute covered by a cooperation agreement with CERN

¹⁴³ Affiliated with an international laboratory covered by a cooperation agreement with CERN.